A juvenile Paleozoic ocean floor origin for eastern Stikinia, Canadian Cordillera

Luke Ootes, Dejan Milidragovic, Richard Friedman, Corey Wall, Fabrice Cordey, Yan Luo, Gabrielle Jones, D. Graham Pearson, Anika Bergen

Research Paper

GEOSPHERE

GEOSPHERE

https://doi.org/10.1130/GES02459.1

14 figures; 1 set of supplemental files

CORRESPONDENCE: Luke.Ootes@gov.bc.ca

CITATION: Ootes, L., Milidragovic, D., Friedman, R., Wall, C., Cordey, F., Luo, Y., Jones, G., Pearson, D.G., and Bergen, A., 2022, A juvenile Paleozoic ocean floor origin for eastern Stikinia, Canadian Cordillera: Geosphere, https://doi.org/10.1130/GES02459.1.

Science Editor: Andrea Hampel
Associate Editor: G. Lang Farmer

Received 9 June 2021
Revision received 22 February 2022
Accepted 14 March 2022

Published online 12 May 2022

A juvenile Paleozoic ocean floor origin for eastern Stikinia, Canadian Cordillera

Luke Ootes[1], Dejan Milidragovic[2], Richard Friedman[3], Corey Wall[3], Fabrice Cordey[4], Yan Luo[5], Gabrielle Jones[5], D. Graham Pearson[5], and Anika Bergen[6]

[1]British Columbia Geological Survey, Ministry of Energy, Mines and Low Carbon Innovation, Victoria, British Columbia V8W 9N3, Canada
[2]Geological Survey of Canada, Vancouver, British Columbia V6B 5J3, Canada
[3]Pacific Centre for Geochemical and Isotopic Research, The University of British Columbia, Earth Sciences Building, 2020–2207 Main Mall, Vancouver, British Columbia V6T 1Z4, Canada
[4]Laboratoire de Géologie de Lyon, Terre Planètes Environnement, Université Claude Bernard Lyon 1, Villeurbanne 69622, France
[5]Department of Earth & Atmospheric Sciences, 1-26 Earth Sciences Building, University of Alberta, Edmonton, Alberta T6G 2E3, Canada
[6]Abandoned Mines Branch, Ministry of Energy, Mines and Low Carbon Innovation, Victoria, British Columbia V8W 9N3, Canada

ABSTRACT

The Cordillera of Canada and Alaska is a type example of an accretionary orogen, but the origin of some terranes remains contentious (e.g., Stikinia of British Columbia and Yukon, Canada). Presented herein are igneous and detrital zircon U/Pb-Hf and trace-element data, as well as the first radiolarian ages from the Asitka Group, the basement to eastern Stikinia. The data are used to evaluate the role of juvenile and ancient crust in the evolution of Stikinia and the tectonic environment of magmatism. Two rhyolites are dated by U-Pb zircon at 288.64 ± 0.21 Ma and 293.89 ± 0.31 Ma, with εHf(t) = +10. Red chert contains radiolarians that are correlated with *P. scalprata* m. *rhombothoracata* + *Ruzhencevispongus uralicus* assemblages (Artinskian–Kungurian). Detrital zircon U/Pb-Hf from a rare Asitka Group sandstone have a mode at ca. 320 Ma and εHf(t) +10 to +16; the detrital zircon suite includes five Paleoproterozoic zircons (~5% of the population). Detrital zircons from a stratigraphically overlying Hazelton Group (Telkwa Formation) volcanic sandstone indicate deposition at ca. 196 Ma with zircon εHf(t) that are on a crustal evolution line anchored from the Asitka Group.

Zircon trace-element data indicate that the Carboniferous detrital zircons formed in an ocean arc environment. The Proterozoic detrital zircons were derived from a peripheral landmass, but there is no zircon εHf(t) evidence that such a landmass played any role in the magmatic evolution of eastern Stikinia. The data support that eastern Stikinia formed on Paleozoic ocean floor during the Carboniferous to early Permian. Consistent with previous fossil modeling, zircon statistical comparisons demonstrate that Stikinia and Wrangellia were related terranes during the Carboniferous to Permian, and they evolved separately from Yukon-Tanana terrane and cratonic North America.

Luke Ootes https://orcid.org/0000-0002-1173-8049

INTRODUCTION

Detrital zircon geochronology is a powerful tool for evaluating the paleogeographic and tectonic history of a region by determining the ages of rocks being eroded during sedimentation. Pairing U-Pb ages with Hf isotopic compositions of zircon allows insights into the origin of the source rocks, particularly those that are poorly preserved (e.g., Pecha et al., 2016). In the Cordilleran orogen of western Canada and Alaska, such data have proven critical to understanding the evolution of constituent terranes, and most terranes now have robust detrital zircon U/Pb-Hf data sets (e.g., Beranek et al., 2013; Malkowski and Hampton, 2014; Colpron et al., 2015; Pecha et al., 2016; Romero et al., 2020; Alberts et al., 2021).

Stikinia, the largest suspect terrane in the northern Cordilleran orogen (Fig. 1; Colpron et al., 2007) comprises mostly Upper Triassic to Lower Jurassic volcanic, sedimentary, and intrusive rocks (e.g., Logan and Mihalynuk, 2014). George et al. (2021) presented the first detrital zircon U/Pb-Hf data set for Upper Triassic to Lower Jurassic sedimentary rocks in western Stikinia. The basement to these rocks, the Stikine assemblage, comprises Devonian through Permian supracrustal and intrusive rocks but is poorly preserved and exposed (Monger, 1977; Brown et al., 1991, 1996; McClelland, 1992; Logan et al., 2000; Gunning et al., 2006a, 2006b, 2007). Although understanding this basement and its antiquity has a bearing on Cordilleran terrane models, proto–Pacific Ocean (Panthalassa) evolution, and porphyry Cu-Au endowment of Stikinia (Fig. 1; Logan and Mihalynuk, 2014), paired zircon U/Pb-Hf data have hitherto been lacking.

The Asitka Group is the deepest exposed basement in eastern Stikinia. Previously identified fossils indicate deposition during the early Permian (e.g., Ross and Monger, 1978), and mudstone, phyllite, and chert indicate a deep-marine environment. During bedrock mapping, rare rhyolite and sandstone units were identified within the southern-most exposures of the Asitka Group (Ootes et al., 2020a, 2020b). We present the first igneous and detrital zircon U/Pb-Hf data from Stikine basement. We pair these data with zircon trace-element data, the advent of which allows for tectonic discrimination of the zircon source (Grimes et al., 2015). This study includes the first radiolarian ages from cherts in the Asitka Group; the biometric and radiometric results refine the timing of Asitka Group deposition. Included are Hazelton Group sandstone (Telkwa Formation; Lower Jurassic) detrital zircon U/Pb-Hf and trace-element data. The zircon εHf(t) and trace-element data are used to evaluate the role of primitive and ancient crust in the evolution of Stikinia and the tectonic environment of parental magma crystallization, enabling comparison to other terranes in the Cordilleran orogen.

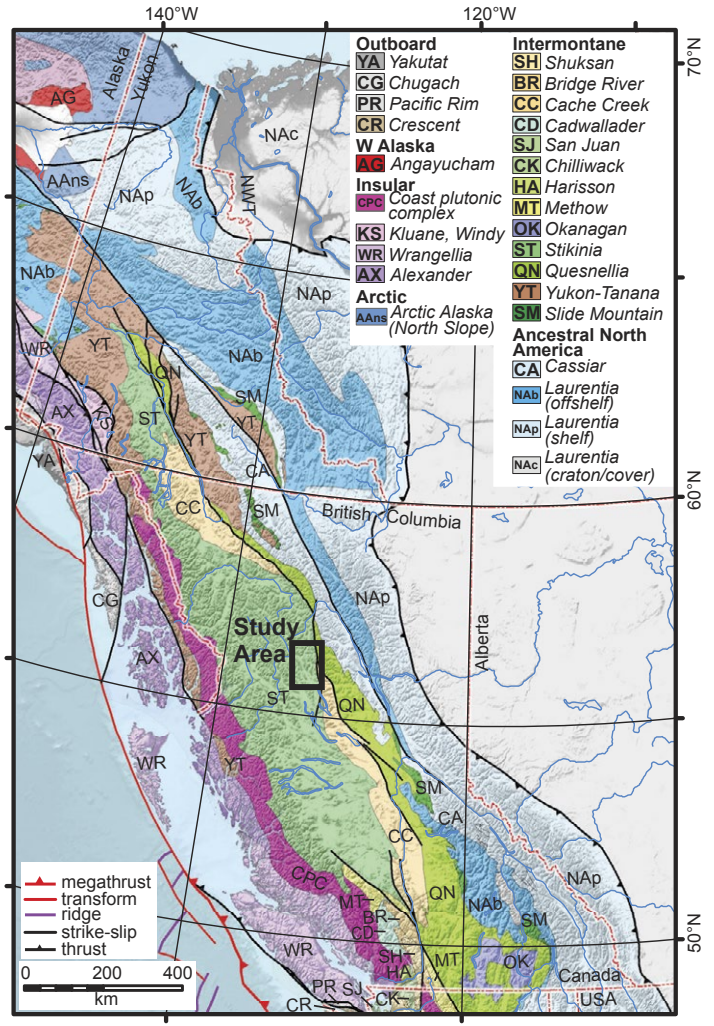

Figure 1. Terrane map of the Cordilleran orogen and the location of this study. After Colpron (2020).

REGIONAL GEOLOGY

The northern Cordilleran orogen of western Canada and Alaska is a collage of parautochthonous and allochthonous terranes. The parautochthonous group of terranes originated as part of the Laurentian margin, whereas the allochthonous group of terranes has paleogeographic affinities from peri-Laurentia to Panthalassa to Baltica (Colpron and Nelson, 2021). Stikinia, part of the classical Intermontane morphological belt, is the largest accreted terrane in the Cordilleran orogen (Monger et al., 1982). It is preserved between Yukon-Tanana and Alexander terranes to the west and Cache Creek and Quesnellia terranes to the east (Fig. 1). Accretion of allochthonous terranes began in the Late Triassic and continued through the Jurassic and involved complex collisional processes between the allochthonous and the parautochthonous terranes (Mihalynuk et al., 1994; Logan and Mihalynuk, 2014; Colpron et al., 2015; Golding, 2020). The relationship between Stikinia and Yukon-Tanana terrane is ambiguous; some consider that Yukon-Tanana terrane is basement to Stikinia (e.g., Jackson et al., 1991; Mihalynuk, 1999), whereas others suggest the terranes remained separate until Mesozoic collision (e.g., Currie and Parrish, 1993; George et al., 2021).

Stikinia comprises a series of unconformity-bounded successions including upper Paleozoic basement rocks of the Stikine assemblage and Asitka Group (Fig. 2; Brown et al., 1991, 1996; McClelland, 1992; Logan et al., 2000; Gunning et al., 2006a, 2006b, 2007), Late Triassic rocks of the Takla, Stuhini, and Lewes River groups (e.g., Monger, 1977; Brown et al., 1996; Logan et al., 2000; Miller et al., 2020; Greig et al., 2021), and Late Triassic to Middle Jurassic rocks of the Hazelton Group (e.g., Tipper and Richards, 1976; Marsden and Thorkelson, 1992; Thorkelson et al., 1995; Gagnon et al., 2012; Barresi et al., 2015; Nelson et al., 2018; Greig et al., 2021). The Late Triassic to Jurassic volcano-sedimentary rocks formed in a suprasubduction zone setting (e.g., Barresi et al., 2015) and are volumetrically the most significant component of Stikinia. All of the supracrustal units have been intruded by plutonic suites, many of which contain porphyry Cu-Au mineralization (e.g., Logan and Mihalynuk, 2014).

The Stikine assemblage includes the oldest stratified rocks in Stikinia (Early Devonian to middle Permian) and forms the basement of western Stikinia. This basement is a mixed carbonate and volcanic succession with minor interbedded siliciclastic rocks (Fig. 2; Monger, 1977; Brown et al., 1991, 1996; McClelland, 1992; Logan et al., 2000; Gunning et al., 2006a, 2006b, 2007). In eastern Stikinia, Paleozoic basement is referred to as the Asitka Group (Figs. 3–5). It comprises felsic-intermediate

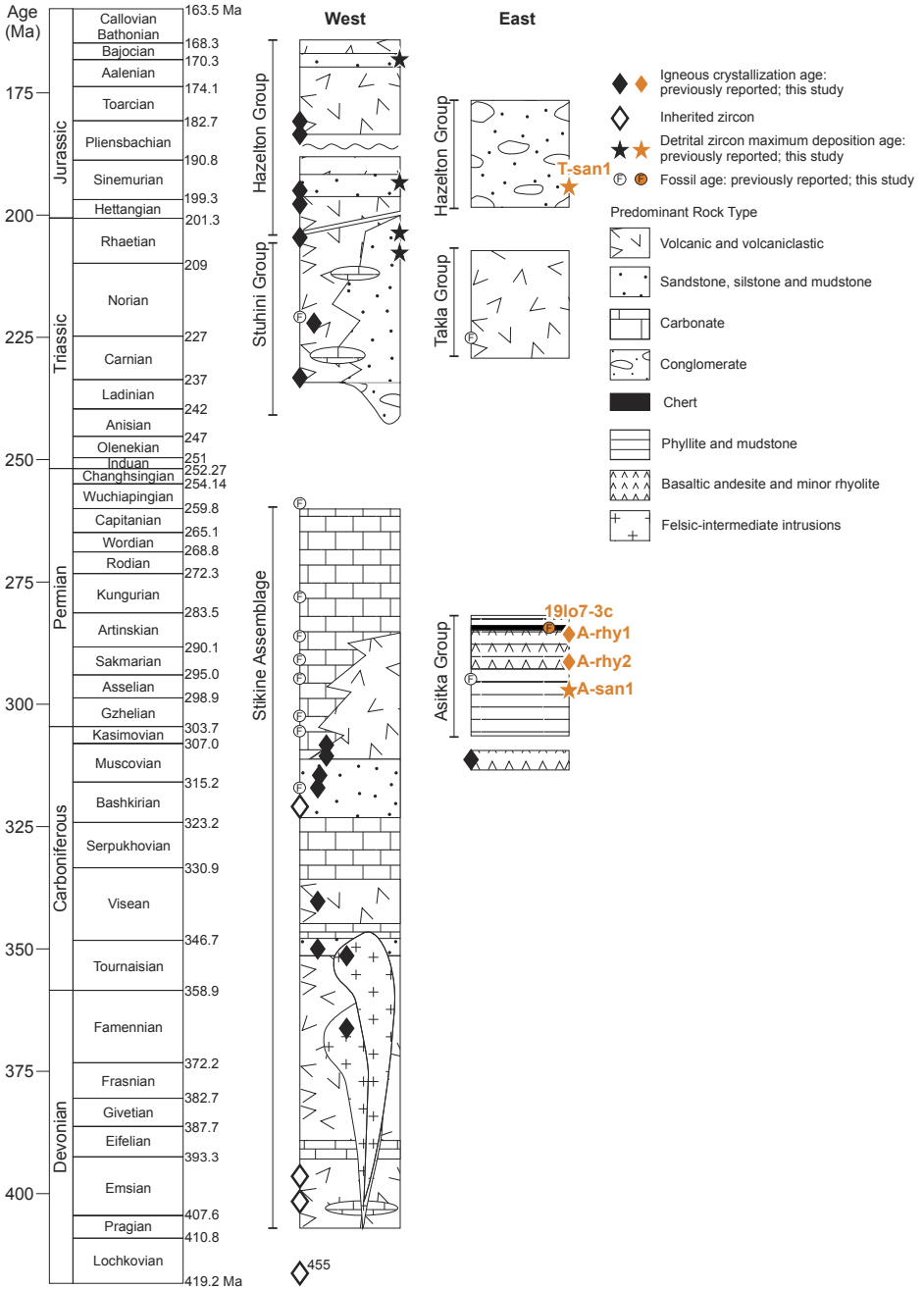

Figure 2. Generalized composite stratigraphy and published geochronology of Stikinia. Western Stikinia is simplified from Brown et al. (1991, 1996), McClelland (1992), Logan et al. (2000), Gunning et al. (2007), Miller et al. (2020), George et al. (2021), and Greig et al. (2021). Eastern Stikinia is constructed from Lord (1948), Monger and Church (1977), Richards (1976), Tipper and Richards (1976), Monger (1977), Diakow (2001), Evenchick et al. (2007), Ootes et al. (2020a, 2020b), and this study. Geological time chart is after Cohen et al. (2013).

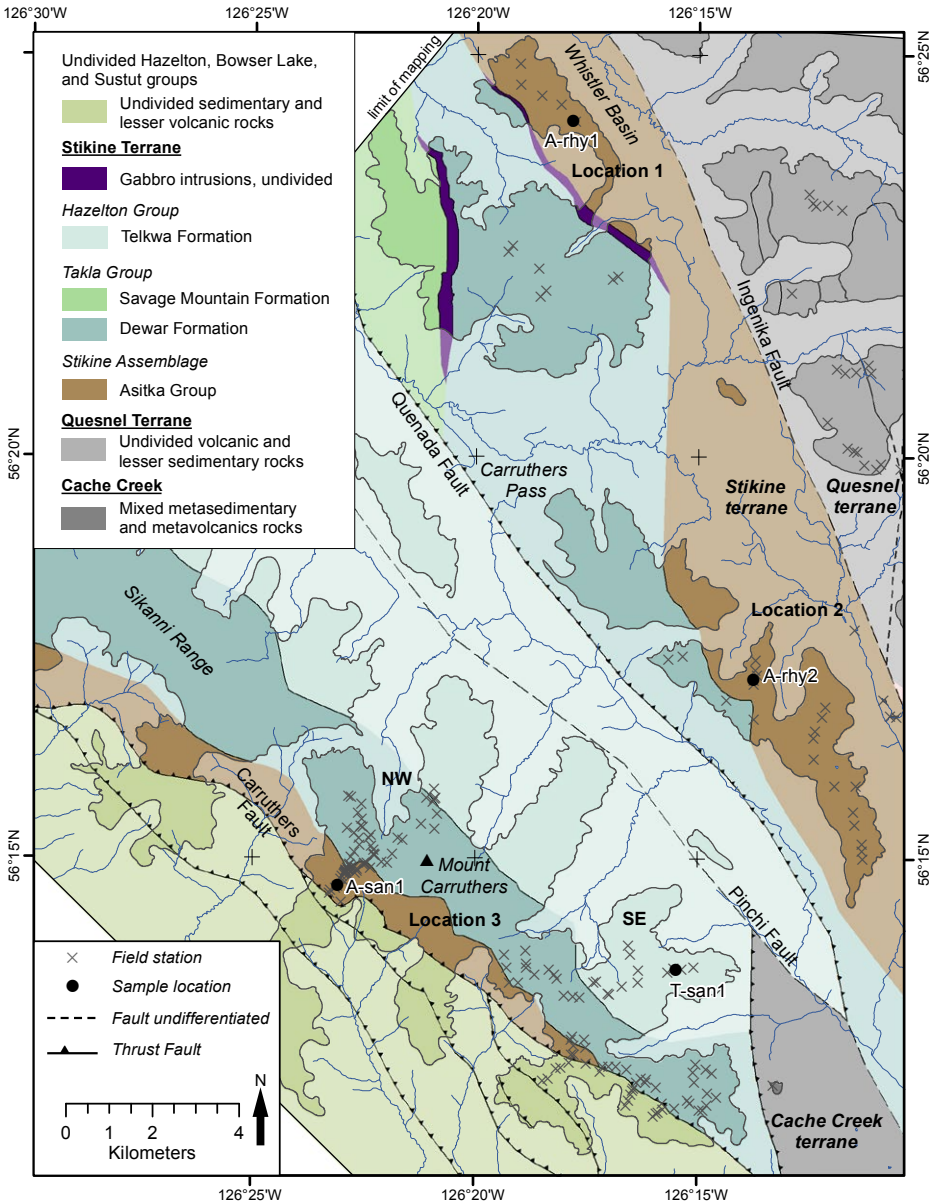

Figure 3. Geological map of the study area in eastern Stikinia. The darker tinted hues are areas of bedrock exposure, and lighter tinted hues are areas of surficial cover. Locations 1, 2, and 3 are identified. Location 3 is subdivided into northwest (NW) and southeast (SE) sections. Simplified after Lord (1948), Richards (1976), Evenchick et al. (2007), and Ootes et al. (2020a, 2020b).

volcanic flows and tuffs, argillite, mudstone, limestone and dolostone, and chert (Lord, 1948; Monger, 1977; Ootes et al., 2020a, 2020b). Although the base of the Asitka Group is not exposed, Lord (1948) suggested a minimum thickness of 2600 m (8500 ft). Fossils, including fusulinids, brachiopods, bryozoa, and sponges indicate it was deposited during the Asselian to Artinskian stages of the Permian (Lord, 1948; Rigby, 1973; Monger, 1977; Ross and Monger, 1978). Paleomagnetic data from Asitka Group volcanic rocks indicate deposition at ~21° to 23°N (Irving and Monger, 1987). Biostratigraphic and sedimentological constraints of the Stikine assemblage (western Stikinia) indicate similar paleolatitudes (Gunning et al., 2006a).

Mafic volcanic and associated sedimentary rocks of the Stuhini Group (western Stikinia) and Takla Group (eastern Stikinia) were deposited disconformably on the Paleozoic basement during the Late Triassic (Lord, 1948; Monger, 1977; Brown et al., 1991, 1996; Logan et al., 2000; Miller et al., 2020; George et al., 2021; Greig et al., 2021). In eastern Stikinia, siliciclastic rocks of the Dewar Formation are the lowest part of the Takla Group. The Dewar Formation is overlain and intercalated with mafic flows and pyroclastic rocks of the Savage Mountain Formation, which is capped by mainly coarse-grained volcaniclastic rocks of the Moosevale Formation (Monger and Church, 1977; Monger, 1977). The Takla Group has not been radiometrically dated, but fossil evidence indicates it is, in part, upper Carnian to Norian and time-equivalent to the Stuhini Group in western Stikinia (Fig. 2; Monger and Church, 1977; Monger, 1977; Logan et al., 2000; George et al., 2021; Greig et al., 2021).

The Takla Group is overlain by the Hazelton Group (Sinemurian to Toarcian; e.g., Tipper and Richards, 1976) in both eastern and western Stikinia (Fig. 2). In eastern Stikinia, the Hazelton Group includes three formations (from base to top: the Telkwa, Nilkitkwa, and Smithers; Tipper and Richards, 1976; Monger, 1977), whereas in western Stikinia, further subdivisions have been detailed (e.g., Nelson et al., 2018). Only the Telkwa Formation was examined in the present study area, where it comprises volcaniclastic rocks, mostly pebble to cobble conglomerates and interbedded mudstone

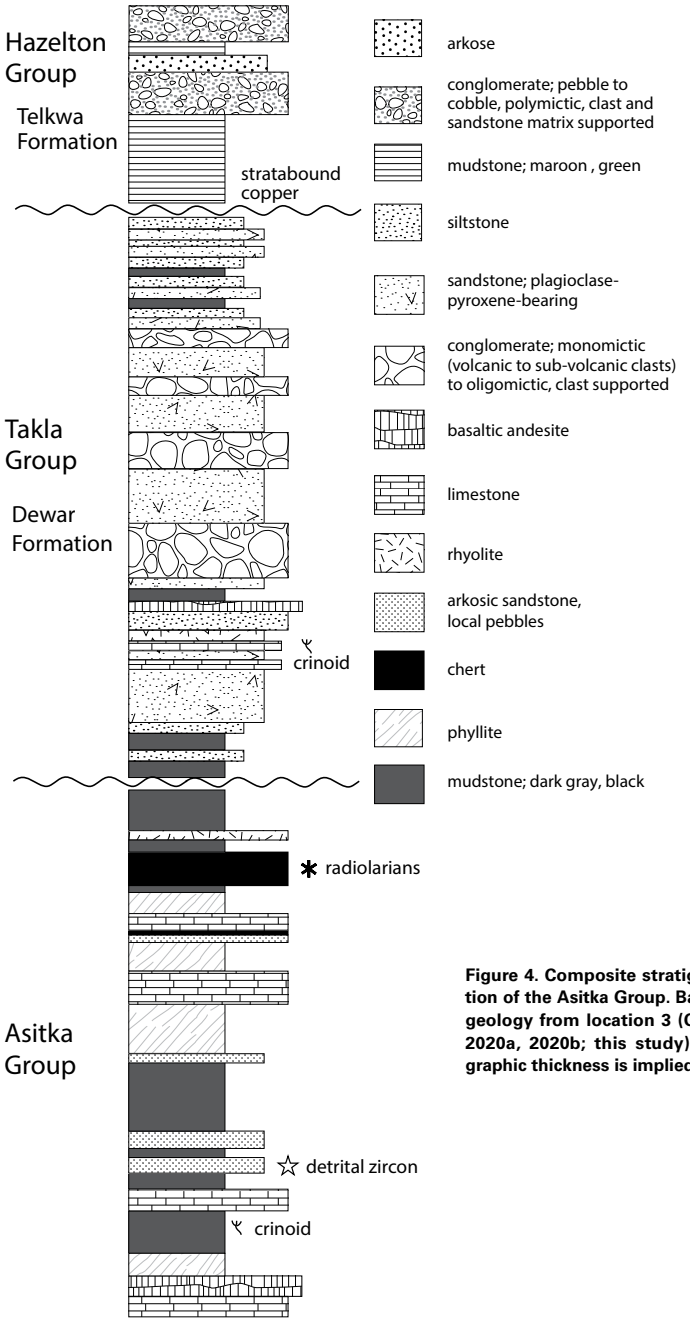

Figure 4. Composite stratigraphic section of the Asitka Group. Based on the geology from location 3 (Ootes et al., 2020a, 2020b; this study). No stratigraphic thickness is implied.

that alternate between maroon and pale-green weathering. These rocks were assigned to the Sikanni facies of the Telkwa Formation by Tipper and Richards (1976). In western Stikinia, the Telkwa Formation is biometrically and radiometrically dated between 205 and 194 Ma (e.g., Barresi et al., 2015). In eastern Stikinia, fossil evidence indicates deposition in the Sinemurian (Fig. 2; Tipper and Richards, 1976; Monger, 1977). Paleolatitudes for the Takla and Hazelton groups indicate deposition between ~23° and 42°N (Monger and Irving, 1980).

STUDY AREA

This study investigated the most southerly exposures of the Asitka Group where it is overlain by the Dewar Formation (Takla Group) and the Telkwa Formation (Hazelton Group; Figs. 1 and 3–5; Lord, 1948; Monger and Church, 1977; Richards, 1976; Tipper and Richards, 1976; Monger, 1977; Evenchick et al., 2007; Ootes et al., 2020a, 2020b). These units are in fault contact with Cache Creek terrane to the east, and both the Stikinia and Cache Creek rocks are juxtaposed with supracrustal and intrusive rocks of the Quesnel terrane along the dextral strike-slip Pinchi-Ingenika fault (Fig. 3). To the west, the Stikine rocks are covered or are in fault contact with younger Hazelton, Bowser Lake, and Sustut group volcano-sedimentary rocks (Jurassic to Cretaceous; Fig. 3; Lord, 1948; Richards, 1976; Evenchick et al., 2007).

All Stikinian rocks in the study area contain two generations of ductile deformation fabrics. The first generation is most prominent as a moderate to strong foliation (S_1) that is typically bedding (S_0) parallel. The second generation is a locally developed cleavage (S_2) that is axial planar to folds (F_2; Ootes et al., 2020b). Ductile deformation postdated deposition of the Telkwa Formation (i.e., <190 Ma).

Asitka Group (Permian)

In the study area, the Asitka Group was examined at three isolated mountains (Fig. 3). Although the stratigraphy at each location differs in detail,

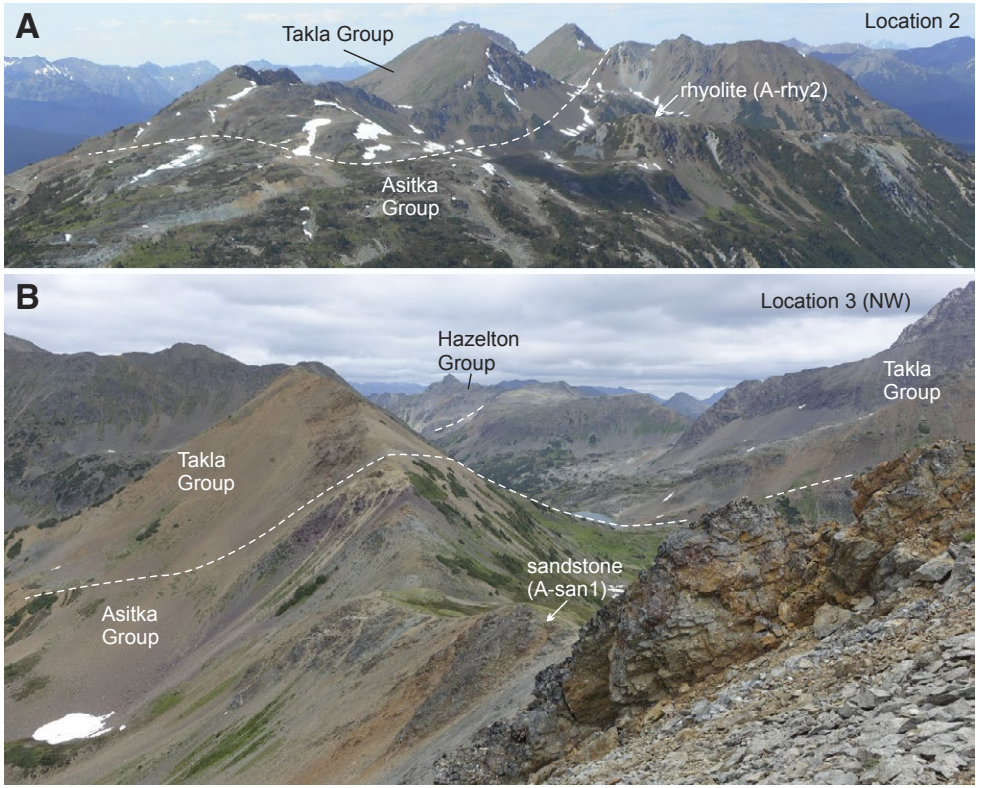

Figure 5. (A) Bedrock exposure at location 2 showing the Asitka Group and Takla Group (Dewar Formation). At this location, the relationship between the two groups, be it structural or stratigraphic, is not constrained. Location of rhyolite sample (A-rhy2) is identified. View is toward the north. (B) The northwest exposure of location 3 showing the continuous stratigraphic section from Asitka, to Takla (Dewar Formation), to Hazelton (Telkwa Formation) groups. Sandstone sample (A-san1) is highlighted. Red chert occurs immediately below the Asitka Group-Takla Group depositional contact, which is not exposed. View is toward the east-northeast.

rock types common to all include chert, phyllite, and basaltic andesite.

At location 1, the Asitka Group is on an isolated plateau immediately west of the Ingenika fault and Whistler Basin (Fig. 3). Younging indicators are lacking, and the Asitka-Takla contact is not exposed. The plateau is mostly basaltic andesite, and other rock types (chert, phyllite) are mostly limited to cliff exposures. In the southern part of the plateau, however, a unit of red and white chert is preserved. The chert unit appears to be >10 m thick, although it is folded and structurally thickened. Adjacent to the chert is ~2 m of mudstone, which is in contact with a 30 cm-thick, fine-grained rhyolite unit that can be traced along strike for 5 m (Fig. S1[1]). The rhyolite has relict spherulite features observable in thin section (Fig. S6A).

[1]Supplemental Material. Contains analytical techniques for zircon U-Pb, Hf, and trace elements; tables with sample locations and analytical results; and figures. Please visit https://doi.org/10.1130/GEOS.S.19449827 to access the supplemental material, and contact editing@geosociety.org with any questions.

Location 2 is west of the Ingenika fault, 12 km southeast of location 1 (Fig. 3). There, the Asitka Group is exposed on three isolated ridgelines; only the southern two were investigated (Figs. 3 and 5A). Again, younging indicators are lacking, and the Asitka-Takla (Dewar Formation) contact is not exposed; it remains unclear if the contact is stratigraphic or structural. The southernmost ridgeline is mostly basaltic andesite; on its northeast flank are mudstones overlain by white ribbon chert. The central ridgeline consists of fragmental rhyolite on the west and lesser basaltic andesite on the east (Fig. S2, footnote 1). The fragmental rhyolite alternates from white to red weathering, indicating differing oxidation states. The clasts are all felsic volcanic and range from lapilli to bomb size. Some fragments or pseudo-fragments appear to be welded, but deformation precludes distinguishing between an epiclastic or pyroclastic origin (Figs. S2B and S2C). Above and east of the rhyolite is massive basaltic andesite. The western edge of the outcrop contains a fine-grained gray limestone unit interbedded with minor amounts of basaltic andesite (Fig. S2C).

The most complete stratigraphic section in the study area is in the Sikanni Ranges at Mount Carruthers (location 3), ~10 km southwest of location 2 (Figs. 3–5). The section youngs to the northeast, from Asitka Group to the Dewar Formation to the Telkwa Formation (Figs. 3–5B; Monger, 1977; Ootes et al., 2020a, 2000b), and mapping results were used to build the composite stratigraphic section (Fig. 4). The Asitka Group is thickest in the northwest part of the section and is structurally cut out to the southeast (Fig. 3). The lower part of the section includes carbonate rocks and basaltic andesite (Fig. 4). These rocks pass upsection to gray and beige phyllite and beige and black mudstone (Fig. S3A), locally containing silicified echinoderms (crinoids). The mudstones are locally interlayered with beds of carbonate and sandstone (up to 4 m thick) that contain quartz and lithic pebbles (Fig. S6B). Above the mudstone is green and steel-gray phyllite with carbonate beds and local thin feldspathic sandstone beds. Red to maroon and locally black chert are above the phyllite and contain radiolarians. The top of the section consists

of maroon, gray, and beige mudstone, phyllite, and carbonate rock (Figs. 4 and S3).

Takla Group—Dewar Formation (Triassic)

Along the length of the Sikanni Range (location 3; Fig. 3; Monger, 1977), the Dewar Formation was deposited on different lithological units of the Asitka Group, indicating the contact is an angular unconformity (Fig. 4). The unconformity is nowhere exposed; at the southeast exposure of location 3, the base of the Dewar Formation is an ~1-m-thick black graphitic mudstone (Fig. S4A), and the unconformity is hidden by a talus-covered interval of ~2 m. The remaining lower part of the Dewar Formation comprises black and brown locally pyritic mudstone and siltstone and rare mafic volcanic rocks (Figs. 4 and S4B). The middle part of the section is mostly medium- to coarse-grained sandstone containing plagioclase and pyroxene. Individual beds are up to 2 m thick and are both massive and cross-bedded. The sandstones commonly have green argillaceous interbeds with well-preserved primary sedimentary structures (e.g., laminations, flame structures; Fig. S4C). Interleaved with the sandstones are monomictic and oligomictic clast-supported pebble and cobble conglomerate beds (Figs. 4 and S4D). Clasts range from well-rounded to subangular. The uppermost part of the Dewar Formation is black mudstone and siltstone with thin (<10 cm), fine-grained feldspathic sandstone beds (Fig. 4). From north of location 3 in the Sikanni Range, bivalve fossils (*Halobia*) in the Dewar Formation are interpreted by Monger (1977) as upper Carnian to lower Norian (ca. 227 Ma).

Hazelton Group—Telkwa Formation (Jurassic)

The Telkwa Formation was only investigated at location 3, in the Sikanni Range (Figs. 3 and 4). The depositional contact with the Dewar Formation has not been directly observed but has been interpreted as an erosional unconformity (Tipper and Richards, 1976; Monger, 1977). In part, this is because the Moosevale and Savage Mountain formations (Takla Group) are missing in the southeast section and interpreted as eroded before Telkwa Formation deposition (Monger, 1977). In the study area, the lower part of the Telkwa Formation includes alternating pale-green and maroon and/or mauve mudstone (Figs. S5A and S5B, footnote 1). Above are heterogeneous siliciclastic rocks that include monomictic to polymictic, pebble and cobble conglomerates that are both clast and matrix supported (Fig. S5C). The clast compositions vary but are typically feldspar-rich and of the volcanic porphyry type. The conglomerates have interbeds that include purple sandstone and green and maroon mudstone (Fig. S5).

Tipper and Richards (1976) and Monger (1977) interpreted the volcaniclastic and epiclastic conglomerate and sandstone as non-marine, assigning them to the Sikanni facies of the Telkwa Formation. The Sikanni facies is not fossil bearing, but correlation to other fossil-bearing rocks of the Telkwa Formation to the south indicates a Sinemurian (199.3–190.8 Ma) time of deposition (Tipper and Richards, 1976).

METHODS

Microfossils

For microfossil separation, 5 kg of red chert (sample 19lo7-3c) were collected from the Asitka Group at location 1 (Figs. 3 and S1, footnote 1). To maximize the quality of the microfossils, one sample was selected with specific detection techniques applied to pelagic strata from ophiolites and suture zones, using a strong hand lens and investigating specific microfacies such as argillaceous layers within chert beds (Cordey and Krauss, 1990). Samples were processed at the Laboratoire de Géologie de Lyon (Lyon, France), where radiolarians were extracted by numerous and repetitive leaching of samples with low-concentration hydrofluoric acid (HF). A large number of etchings were required (~20 × 24 or 48 h) due to the recrystallization of the chert, a result of diagenesis and later deformation (Figs. 6 and S1). Radiolarians were handpicked and mounted on an aluminum stub for scanning electron microscope (SEM) observation and taxonomical identifications (SEM Zeiss Supra 55 VP, Ecole Normale Supérieure de Lyon).

Zircon U/Pb-Hf and Trace-Element Analysis

Two rhyolite samples from the Asitka Group, one from location 1 (A-rhy1) and one from location 2 (A-rhy2; Fig. 3; Table S1, footnote 1), were collected for igneous zircon U/Pb-Hf and trace-element analysis. Two clastic samples were collected for detrital zircon U/Pb-Hf and trace-element analyses from location 3 (Fig. 3). These include an Asitka Group sandstone (A-San1) and a Hazelton Group sandstone (Telkwa Formation; T-san1). Five samples of medium- to coarse-grained plagioclase and pyroxene-bearing sandstone from the Dewar Formation were collected but did not yield zircon through standard mineral separation.

Each sample weighed ~5 kg and was collected from unaltered and lichen-free bedrock. Cathodoluminescence (CL) imaging and zircon U/Pb-Hf and trace-element analyses were completed at the Pacific Centre for Isotopic and Geochemical Research (PCIGR) at the University of British Columbia (Vancouver, British Columbia, Canada) and the Arctic Resources Laboratory (ARL) at the University of Alberta (Edmonton, Alberta, Canada). Results are in Tables S1–S6 (footnote 1), and all analytical techniques and results of data quality control samples are in appendices 3 and 5 in Ootes et al. (2020c).

Igneous zircons were analyzed for U-Pb and trace elements by laser ablation–inductively coupled plasma–mass spectrometry (LA-ICP-MS) at PCIGR (Tables S2 and S3, footnote 1). A subset of the best quality zircon was then selected and analyzed by chemical abrasion–isotope dilution–thermal ionization mass spectrometry (CA-ID-TIMS; Table S5) by techniques modified from Mundil et al. (2004), Mattinson (2005), and Scoates and Friedman (2008). After CA-TIMS, four separate zircons from sample A-rhy2 were selected for Lu-Hf isotopic analysis (Table S6). Zircons were selected based on size, appropriate trace elements (e.g., low Ca, Fe, P, and La), and single zircon $^{206}Pb/^{238}U$ ages were determined by LA-ICP-MS. Zircons were dissolved, and after anion exchange by column chemistry, the Hf isotopic compositions were measured by static multi-collection using a MC-ICP-MS following the methods of Goolaerts et al. (2004) and Weis et al. (2007).

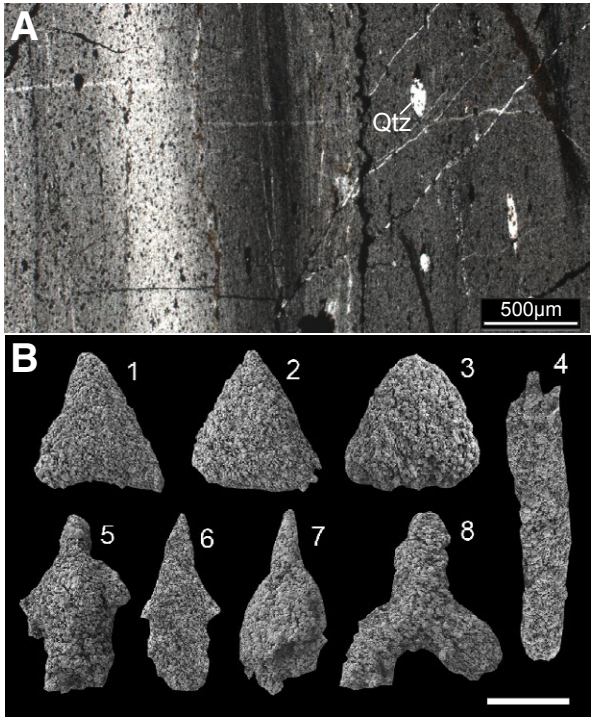

Figure 6. Asitka Group chert. (A) Photomicrograph of chert with local chert nodules (Qtz). (B) Scanning electron microphotographs of radiolarians from the Asitka Group chert. For each picture: radiolarian taxon, scale length (corresponds to white bar at bottom right of image). 1: *Ruzhencevispongus uralicus*, 120 µm; 2–3: *Ruzhencevispongus* spp., 120 µm; 4: arm of *Latentibifistula* sp., 180 µm; 5: *Parafollicucullus scalprata* m. *rhombothoracata*, 120 µm; 6: *Parafollicucullus* sp. cf. *scalprata* m. *rhombothoracata*, 120 µm; 7: *Parafollicucullus* sp., 140 µm; 8: *Latentifistula* sp., 160 µm.

Detrital zircon U-Pb and trace elements were determined by LA-ICP-MS at PCIGR, and Lu-Hf isotopes were determined by LA-MC-ICP-MS at ARL. An additional 35 zircon U/Pb-Hf and trace-element analyses were completed on sample A-san1 at PCIGR (Tables S2–S4).

Zircon Screening

Igneous and detrital zircon data presented in this study (data in the Supplemental Material, footnote 1) were screened based on trace-element results. This screening was completed to avoid data that may include mineral inclusions (e.g., apatite) intercepted during zircon laser ablation. Previous studies (e.g., Grimes et al., 2015) have commonly screened results based on absolute trace-element values; for example, zircon with >100 ppm Ca. However, if we had chosen this value for the present study, a large amount of the data would have been screened out because of the relatively high Ca contents of Stikinian zircons and high uncertainty attached to the Ca results (Fig. S7A). Instead, we adopted a modified approach in which the data were plotted and the outliers identified and removed. This approach used Ca, ^{57}Fe, P, Ti, La, and Ce (Fig. S7). Some minor outliers remained (e.g., relatively high P, Ti, and La), but in these, the zircon U/Pb-Hf and other trace-element data are internally consistent relative to other results. An example of the screening results from one detrital zircon sample (A-san1) is presented in Figure 7A. The trace-element screening procedure independently identified analyses that have non-typical zircon chondrite-normalized, light rare-earth elements (LREEs). A few analyses with typical zircon chondrite-normalized patterns were also screened out because they contained anomalous concentrations of other trace elements (Fig. 7A); retaining or removing those analyses does not impact the U-Pb or εHf interpretations. The screened-out zircons have comparable ^{238}U/^{206}Pb ages to those with typical zircon trace-element compositions (Fig. S7).

RESULTS

Microfossils

The radiolarian fauna in the chert of the Asitka Group are poorly preserved due to postdepositional silica recrystallization and deformation (Fig. 6). While this hinders species-level identification, the following radiolarian taxa were identified: *Latentibifistula* sp., *Latentifistula* sp., *Parafollicucullus* sp. cf. *scalprata* m. *rhombothoracata* (Ishiga and Imoto), *Ruzhencevispongus uralicus* Kozur, and *Ruzhencevispongus* spp. (Fig. 6B). This assemblage is correlative with lower Permian *P. scalprata* m. *rhombothoracata* and *Ruzhencevispongus uralicus* assemblages, ranging from the late Artinskian to the late Kungurian (Aitchison et al., 2017).

The paleoenvironment of chert deposition is not well established. The chert differs from typical deep-water ribbon cherts, which consist of up to 80%–90% radiolarian shells that are typically associated with ophiolites. In the Asitka Group, radiolarians only represent 20%–40% of the chert; other components include oxidized ferruginous clays and possibly volcanic jasper. Therefore, the Asitka cherts may represent a mix of both hydrothermal volcanic-related chemogenic and biogenic processes (e.g., Cordey and Cornée, 2009).

Asitka Group Igneous Zircon

A-rhy1

Asitka Group rhyolite A-rhy1 is a fine-grained Asitka Group rhyolite from location 1 (Figs. 3 and S1; Table S1). It is strongly recrystallized, but devitrified spherulite-like features are preserved (Fig. S6A). Sample A-rhy1 yielded ~50–100-µm-long, oscillatory zoned zircon fragments (Ootes et al., 2020c). Fifteen zircons were analyzed by LA-ICP-MS (Tables S2 and

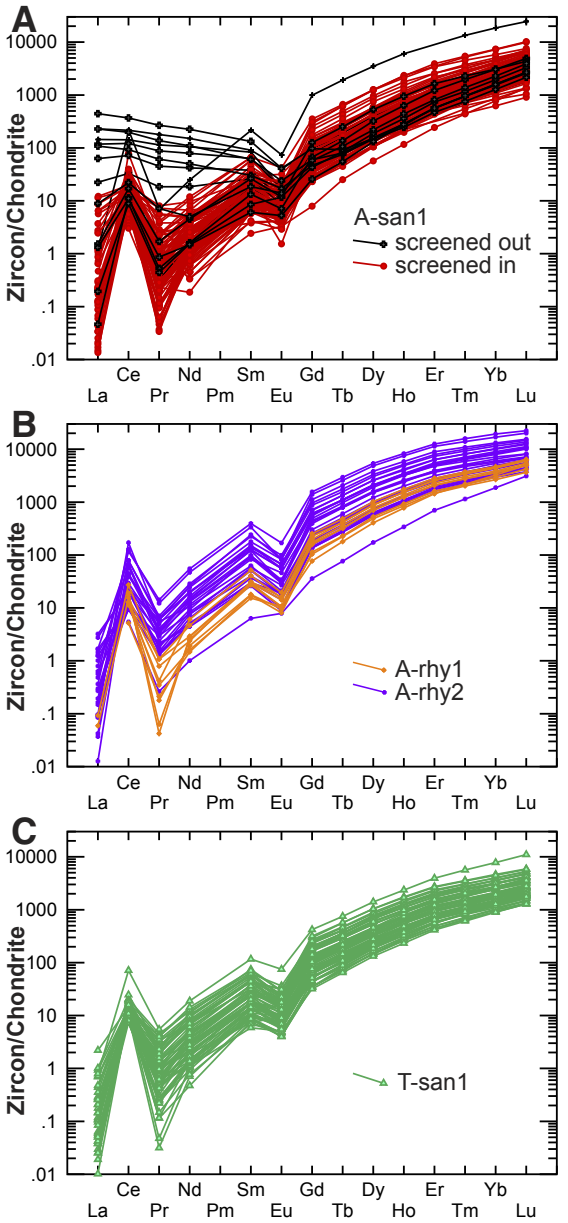

Figure 7. Chondrite-normalized (Sun and McDonough, 1989) rare-earth elements from zircons. (A) Asitka Group sandstone detrital zircons (A-san1). Data in black were independently screened using anomalous Ca, Fe, P, Ti, La, and Yb results (see text for discussion). (B) Asitka Group rhyolite igneous zircons (A-rhy1 and A-rhy2). Screened data are not shown. (C) Telkwa Formation sandstone detrital zircons (T-san1). Screened data are not shown.

S3, footnote 1). Ten zircon results remained after screening using the trace elements (Fig. 7B). From these zircons, six single grains were analyzed by CA-TIMS (Table S5). These grains yielded overlapping concordant ages with a weighted-mean $^{206}Pb/^{238}U$ age of 288.64 ± 0.21 Ma (MSWD = 0.71, probability = 0.62), interpreted as the crystallization age of the rhyolite (Fig. 8A). Zircons from A-rhy1 were considered too small for single-grain, solution-based Lu-Hf analysis.

A-rhy2

A-rhy2 is a strongly deformed Asitka Group fragmental rhyolite from location 2 (Figs. 3, 5A, and S2; Table S1). The sample yielded <100–200-µm-long oscillatory zoned zircon fragments (Ootes et al., 2020c). Forty zircons were analyzed by LA-ICP-MS, and 29 remained after trace-element screening (Tables S2 and S3). Five single zircons were selected and analyzed by CA-TIMS (Table S5). Four results overlap on concordia at ca. 294 Ma, while one zircon yielded a younger $^{206}Pb/^{238}U$ age of 289.6 ± 0.9 Ma (not included in weighted mean) that results from lead loss. The weighted-mean $^{206}Pb/^{238}U$ age from the four zircons (293.89 ± 0.31 Ma; mean square of weighted deviates [MSWD] = 1.27, probability = 0.28) is interpreted as the crystallization age of the rhyolite (Fig. 8B).

Four zircons were selected for Hf isotopic compositions by multi-collector (MC)-ICP-MS (Table S6). The largest zircon (T-1) broke, and the two fragments were analyzed separately. These fragments and one other zircon (2-5) have present-day εHf(0) +6.0 (±0.1; 2SE), +6.3 (±0.2), and +6.4 (±0.2). Two other zircons (3-3 and 3-5) have higher Hf concentrations (Fig. S8) and yield lower εHf(0) of +3.7 (±1.7) and +4.0 (±0.4). The results correspond to time-corrected initial εHf(t) = +9.1 to +11.3 (Figs. S8 and S11; Table S6, footnote 1).

Asitka Group Detrital Zircon

A-san1

Asitka Group sandstone sample A-san1 is from the northwest section of location 3 (Fig. 3; Table S1).

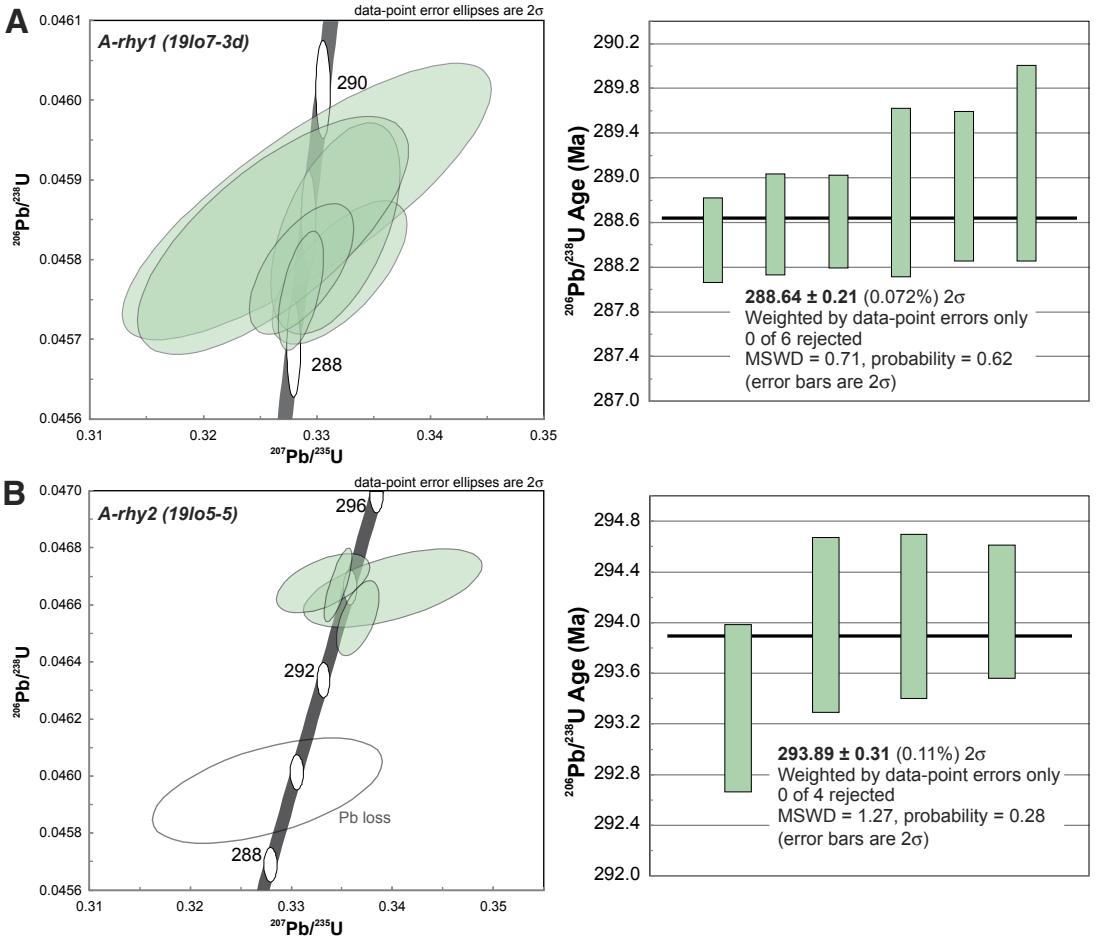

Figure 8. Concordia and $^{206}Pb/^{238}U$ weighted-mean plots of chemical abrasion–thermal ionization mass spectrometry (CA-TIMS) results from Asitka Group igneous zircons from samples (A) A-rhy1 and (B) A-rhy2. MSWD—mean square of weighted deviates.

The sandstone unit is deformed, ~4 m thick, fine to medium grained, and contains quartz and lithic pebbles (Fig. S6B). The unit is near the middle of the Asitka section, where it immediately overlies black mudstone and is overlain by black, brown, and beige mudstone (Figs. 4 and 5B). This is the only quartz-bearing sandstone unit that has been identified in the Asitka Group. One hundred and fifteen prismatic to rounded detrital zircons were analyzed by LA-ICP-MS. Trace-element data indicate that inclusions were encountered in 19 (16.5%) zircons during laser ablation analysis, and these zircons were screened out. The remaining 96 zircons (Tables S2–S4) have typical chondrite-normalized REE patterns (Fig. 7A).

Ninety-one zircons yield a range of $^{206}Pb/^{238}U$ ages between 305.4 ± 7.3 and 354.5 ± 9.4 Ma, and five zircons yield Paleoproterozoic ages with $^{207}Pb/^{206}Pb$ ages ranging from 1647 ± 29–2177 ± 122.2 Ma (Figs. 9A–9D; Table S2). We consider that the maximum deposition age is close to the time of rhyolite eruption at ca. 295 Ma, which is younger than the youngest single zircon age of 305.4 ± 7.3 Ma, and ~20 m.y. younger than the youngest statistical population at 314.8 ± 1.3 Ma (n = 42; MSWD = 1.02; Figs. 9C and S9, footnote 1). This interpretation is supported by previously examined fossil assemblages, including fusulinids, brachiopods, bryozoa, and sponges that indicate the Asitka Group was deposited during the Asselian to Artinskian (Lord, 1948; Rigby, 1973; Monger, 1977; Ross and Monger, 1978). Two-component finite unmixing of the detrital zircon data yields

calculated ages of 318.3 ± 0.7 (77%) and 335.2 ± 1.4 (23%; Fig. 9D).

The Carboniferous detrital zircons from sample A-san1 have present-day εHf(0) from +3.2 to +9.7 (n = 79) with a median at +5.7 (median uncertainty = ±1.4; 2σ), corresponding to εHf(t) from +10.0 to +16.3. The Paleoproterozoic zircons (n = 4) have present-day εHf(0) from 38.7 to –55.4, corresponding to εHf(t) from 9.2–2.3 (Fig. S11; Table S4, footnote 1).

Hazelton Group (Telkwa Formation) Detrital Zircon

T-san1

Telkwa Formation sandstone sample T-san1 is from the southeast section of location 3 (Figs. 3 and 4; Table S1). It is a purple-white, medium-grained, feldspathic sandstone (Figs. S5C and S6d) interbedded with monomictic and polymictic pebble and cobble conglomerate with volcanic clasts, and green and maroon mudstone (Fig. S5). Seventy-eight oscillatory zoned whole zircons and zircon fragments were analyzed by LA-ICP-MS. The trace-element data were used to screen out 11 zircons. The remaining 67 zircons have typical chondrite-normalized REE patterns (Fig. 7C).

The zircons yield a range of $^{206}Pb/^{238}U$ ages from 173.9 ± 5.7 to 206.6 ± 9.2 Ma (Table S2; Ootes et al., 2020c). To estimate the maximum deposition age, data were first tested for discordance. The peak of the probability curve is centered at ca. 196 Ma (Figs. 9E and S10A). The youngest single population (YSP) was estimated using the weighted average of the youngest sub-sample that yielded a mean square of weighted deviates (MSWD) of ~1 (Coutts et al., 2019). The best YSP result is from the second and third youngest zircon ages, which yield a $^{206}Pb/^{238}U$ weighted mean of 178.5 ± 4.3 Ma (MSWD = 1.05; n = 2; Figs. 9E and S10B, footnote 1). However, LA-ICP-MS data can yield ages that are younger than the deposition age (e.g., Herriott et al., 2019). Assuming a single zircon population and using the Tuffzirc function (Ludwig, 2003) yields a 196.15 $^{+1.15}/_{1.35}$ Ma age (Fig. S10C). Unmixing yields two-component calculated ages of 181.3 ± 2.7 Ma (12%) and 197.09 ± 0.96 (88%; Fig. S10D). Using three components (Fig. 9F) yields calculated ages of 180.8 ± 1.3 Ma (2.5%), 195.3 ± 0.8 (66%), and 200.8 ± 1.2 (23%). The older result in the two-component and middle result in the three-component unmixing are indistinguishable from the Tuffzirc result at ca. 196 Ma. These data correspond to correlations (Sinemurian) by Tipper and Richards (1976) and to zircon U-Pb dating of volcanic rocks of the Telkwa Formation in western Stikinia (Barresi et al., 2015; Greig et al., 2021). Whereas Herriott et al. (2019) prefer YSP maximum deposition ages, we interpret the youngest zircons in the Telkwa sandstone to be unreliable, likely from undetected lead loss. We interpret the maximum deposition age as 196 Ma (Fig. 9E), consistent with Sinemurian fossil assemblages (Tipper and Richards, 1976).

Detrital zircons in T-san1 yield a range of present-day εHf(0) from +0.1 to +7.2 (n = 46) with a median +5.2 (±1.5; 2σ). The results correspond to εHf(t) from +4.3 to +11.4 (Fig. S11; Table S4, footnote 1). Notably, the lowest εHf(t) result (4.3 ± 2.3) has the highest total Hf concentration (11380 ± 160 ppm) but overlaps, within uncertainty, the next lowest εHf(t) result (6.3 ± 1.6; Fig. S11).

DISCUSSION

Biostratigraphic and Chronostratigraphic Implications

Cherts from the Asitka Group have *P. scalprata* m. *rhombothoracata* + *Ruzhencevispongus uralicus* radiolarian assemblages (Fig. 6) that are Late Artinskian to Kungurian (<286 to >273 Ma) and slightly younger than the rhyolite (A-rhy1), which yielded a U-Pb zircon crystallization age of 288.64 ± 0.21 Ma (Fig. 10). This radiolarian assemblage supports chert deposition above the volcanic rocks (Fig. S1A), possibly a few million years later. The rhyolite at location 2 yielded a U-Pb zircon age of 293.89 ± 0.31 Ma, and both rhyolite ages are consistent with previously reported Asselian to Artinskian fossil assemblages (Lord, 1948; Rigby, 1973; Monger, 1977; Ross and Monger, 1978).

Ninety-five percent of the Asitka Group sandstone detrital zircons range from 355 to 305 Ma (n = 91; Carboniferous–Middle Mississippian to Middle Pennsylvanian). The results yield a YSP at ca. 315 Ma, and the youngest single grain at ca. 305 Ma (Fig. 9C). However, the maximum deposition age is estimated to correspond with the older ca. 295 Ma rhyolite, and the Asitka Group is interpreted to have been deposited during the Asselian to Kungurian (<298.9 to >273Ma; Fig. 10).

Five Paleoproterozoic zircons (1.65–2.18 Ga) represent ~5% of the detrital zircon data set (Fig. 9A). George et al. (2021) reported poorly defined early Paleozoic to Neoarchean detrital zircons (<3%) from the Stuhini and Hazelton groups in western Stikinia. In contrast, Greig et al. (2021) dated >300 detrital zircons from the Stuhini Group and discovered no zircon older than ca. 225 Ma. George et al. (2021) show that of the pre-Triassic zircons in the Stuhini and Hazelton groups, 90% have a peak probability at 320 Ma (Fig. 10). Based on geological and isotopic arguments, they identified provenance from local Stikine assemblage igneous sources. Western Stikinia contains Early Devonian to Early Mississippian volcanic and intrusive rocks (e.g., Logan et al., 2000) and corresponding inherited zircon in younger intrusions (Miller et al., 2020; Fig. 10), but only few (n = 8) zircons of those ages were discovered by George et al. (2021) from a single Stuhini Group sample. Neither the Stuhini Group sample of Greig et al. (2021) nor the Asitka or Hazelton groups in the present study have Devonian to Early Mississippian zircons. Apparently, Devonian basement source rocks did not exist or were not exposed to erosion in eastern Stikinia during the early Permian.

Zircon U/Pb-Hf

The Asitka Group igneous and detrital zircon εHf(t) data are consistent with derivation from juvenile crust during the Carboniferous to Permian, with no evidence of interaction with or derivation from older continental crust (Fig. 11). In western Stikinia, a minor proportion of detrital zircons from the Stuhini and Hazelton groups are more evolved, indicating minor but detectable influence by older

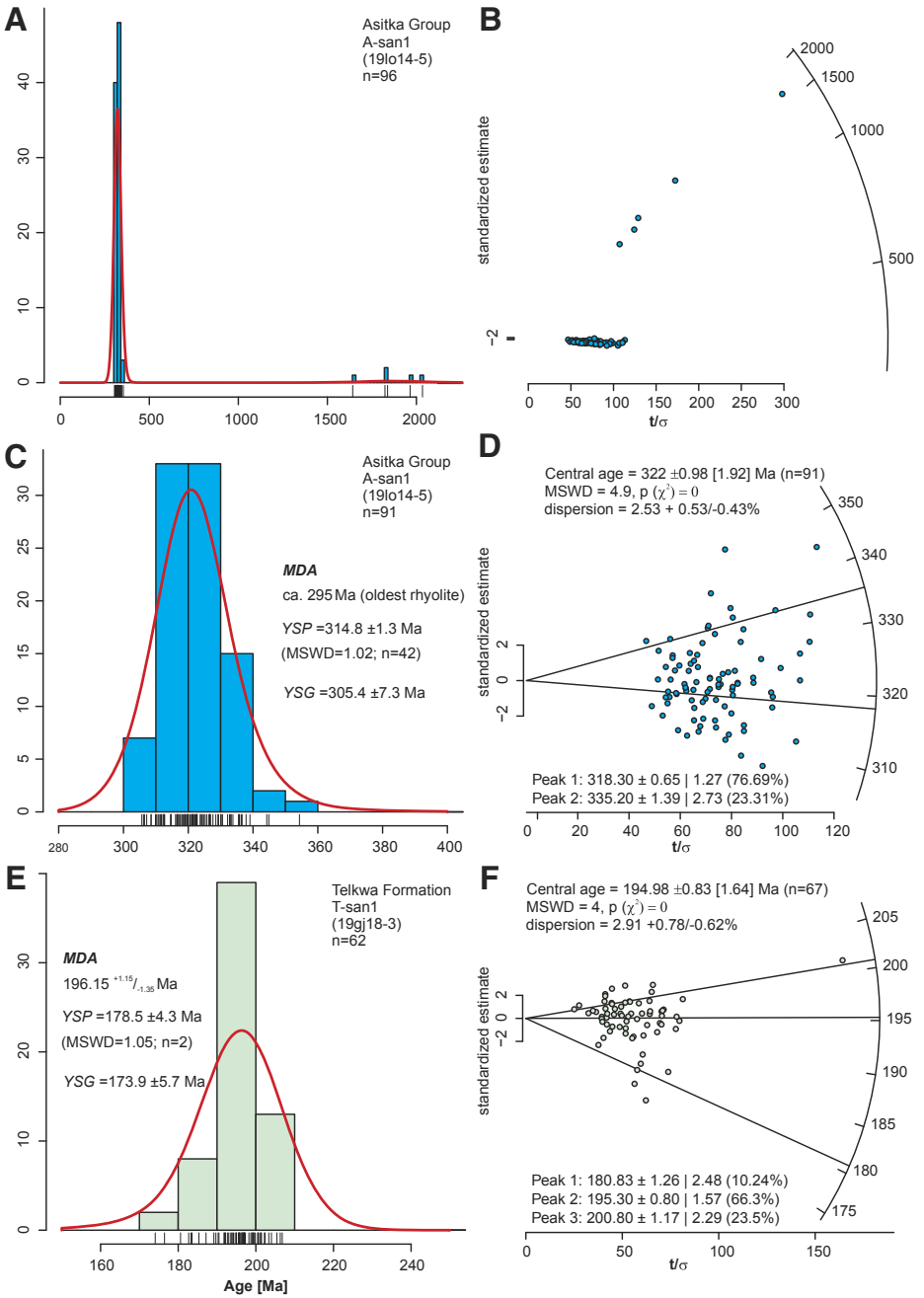

Figure 9. Kernel density element (KDE) and radial plots (Galbraith, 1994) of detrital zircon results. (A) and (B) Asitka Group (A-san1) detrital zircon U-Pb results, including Precambrian results, and (C) and (D) without Precambrian results. Results of two-component finite unmixing are shown on the radial plot. (E) and (F) Hazelton Group (Telkwa Formation) detrital zircon U-Pb results. Results of three-component finite unmixing are shown on the radial plot. MDA—maximum deposition age; YSP—youngest statistical population; YSG—youngest single grain. The KDE and radial plots were generated using IsoplotR (Vermeesch, 2018) where the KDEs have a kernel and histogram bandwidth of 10. See text for discussion of MDA interpretation and data in Supplemental Material (text footnote 1) for supporting results. MSWD—mean square of weighted deviates.

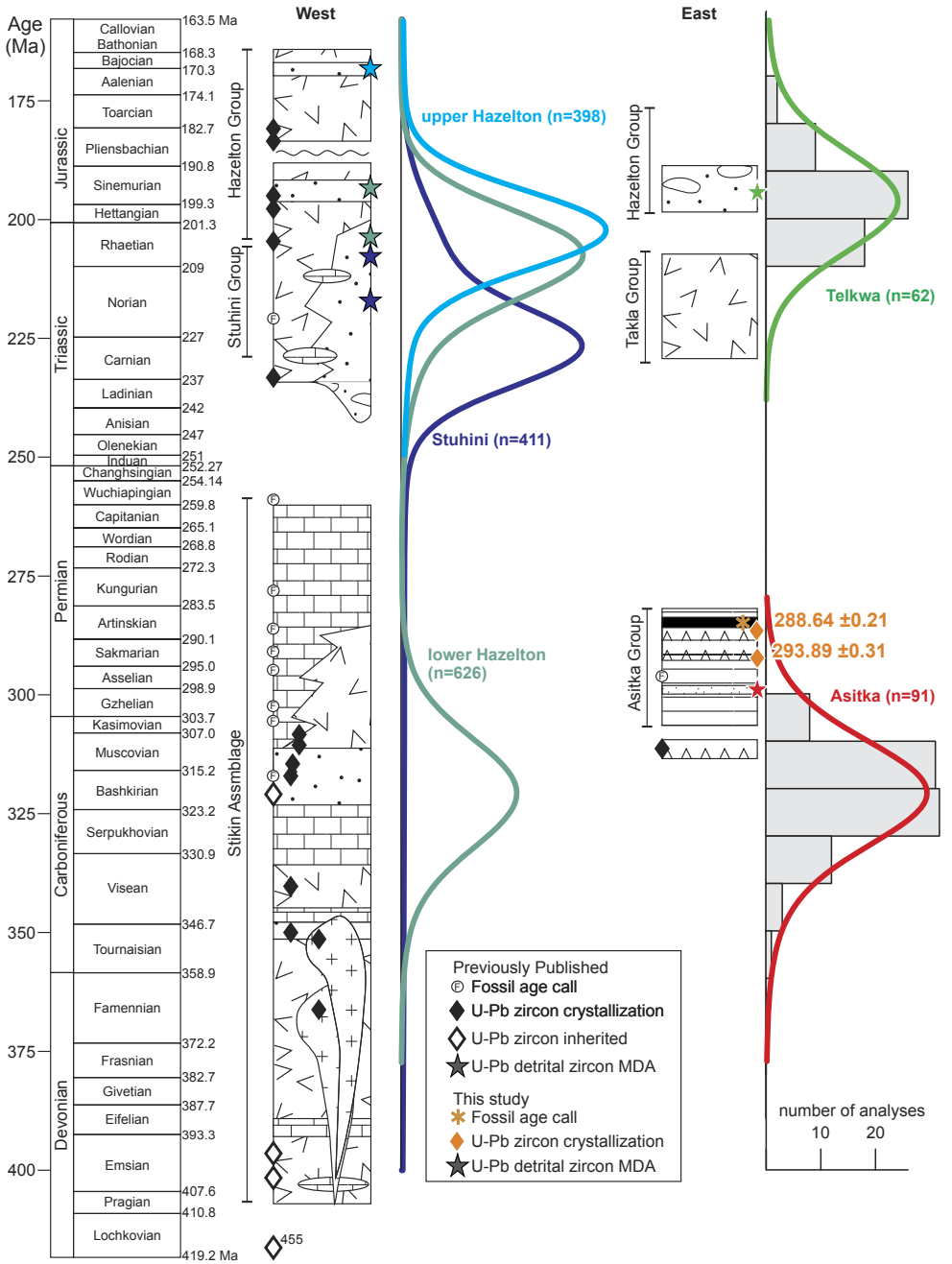

Figure 10. Generalized composite stratigraphy of Stikinia (see Fig. 2 for details) with addition of new detrital zircon U-Pb results. Western Stikinia U-Pb detrital zircon data are from George et al. (2021). MDA—maximum deposition age.

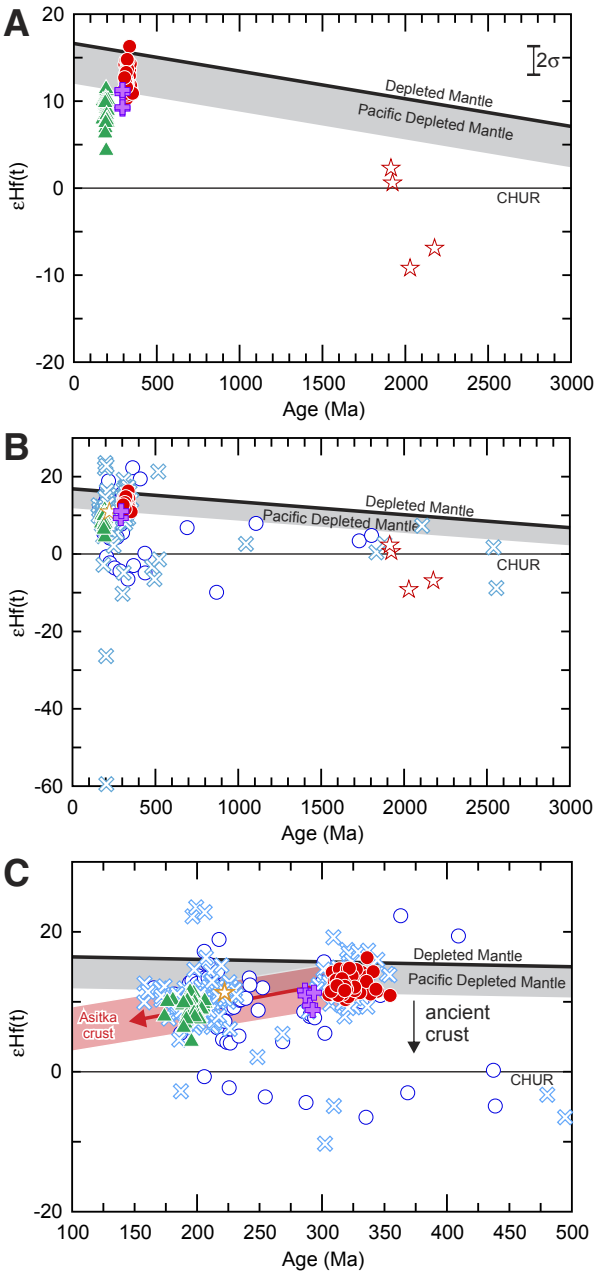

Figure 11. Single zircon U-Pb age versus εHf(t). (A) Asitka Group and Hazelton Group (Telkwa Formation) detrital zircon εHf(t) results. Typical 2σ uncertainty is shown; the Asitka Group rhyolite igneous zircon εHf(t) were determined from solution chemistry and have 2σ uncertainty smaller than the symbol size. (B) and (C) Comparison of eastern Stikinia results (this study) to Stuhini and Hazelton group results from western Stikinia (Milidragovic et al., 2018; George et al., 2021). The red band is the evolution of Asitka Group Carboniferous detrital zircons. CHUR—chondrite uniform reservoir, after Bouvier et al. (2008); depleted mantle and range of Pacific depleted mantle from Chauvel and Blichert-Toft (2001).

crust (Fig. 11B; George et al., 2021). Nonetheless, most detrital zircons from the Stuhini and Hazelton groups lie on the crustal evolution line derived from the Asitka Group (Fig. 11C). The picrite from the Stuhini Group overlaps this crustal evolution line, but its εHf(t) represents mantle values at the time of its eruption (ca. 222 Ma; Milidragovic et al., 2018). The picrite data, combined with the small spread of Asitka Group εHf(t) data, may indicate both normal and enriched mid-ocean ridge basalt (MORB) mantle was involved in the evolution of Stikinia (Milidragovic et al., 2018).

Comparison of zircon U-Pb data indicates eastern Stikinia has a different evolution than Yukon-Tanana terrane but is similar to Wrangellia (Fig. 12A). Figure 12B compares Stikinian zircon U/Pb-Hf (this study; George et al., 2021) with North American basement (Hottah, Davis et al., 2015), Yukon-Tanana terrane (Pecha et al., 2016; Romero et al., 2020), and Wrangellia (Romero et al., 2020; Alberts et al., 2021). Multivariate statistical evaluation of zircon populations younger than 400 Ma (Fig. 12C) demonstrates that eastern Stikinia likely has no relationship with the Yukon-Tanana terrane. The data show that 95% of zircons from western Stikinia overlap with those from eastern Stikinia. The more evolved zircons from western Stikinia could indicate imbrication with Yukon-Tanana or some other evolved terrane in the Late Triassic. The similarity of Carboniferous detrital zircons in Stikinia and Wrangellia samples is remarkable (Fig. 12).

Zircon Trace Elements

The zircon trace elements (Figs. 13, S7, and S11; Table S3, footnote 1) help identify the nature of the underlying crust, be it ocean arc, ocean island basalt (OIB), or MORB. At a given Nb/Yb ratio, the detrital zircons have U/Yb values above the mantle zircon array, most consistent with zircon formation in a predominantly "arc-like" environment, with a negligible contribution of OIB or MORB (Fig. 13; Grimes et al., 2015). Because the Asitka Group has arc-like zircon chemistry and juvenile εHf(t), which does not permit old crust, the environment of zircon crystallization is best interpreted as incipient ocean

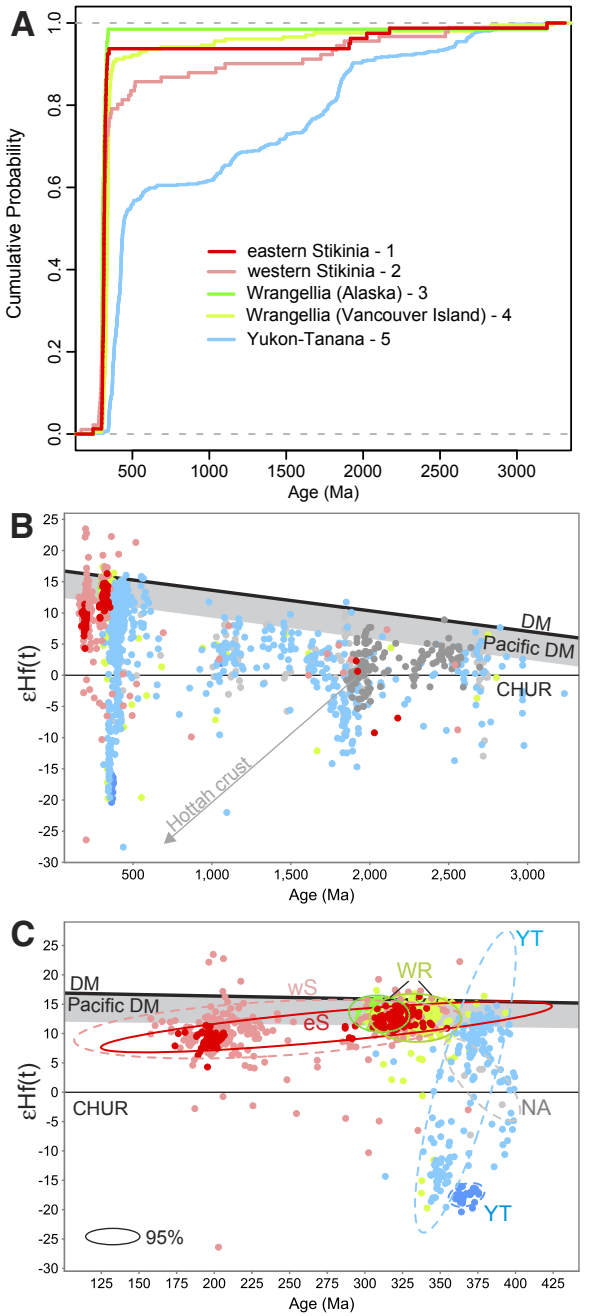

Figure 12. (A) Comparison of cumulative probability of detrital zircons (>300 Ma) from various terranes in the northern Cordilleran orogen. (B) Single zircon age versus εHf(t) for eastern and western Stikinia, Yukon-Tanana, and Wrangellia. Hottah terrane detrital zircon represents the western Canadian Shield before ca. 1.9 Ga (Davis et al., 2015) and its evolution to εHf(0). (C) Single zircon age versus εHf(t) screened to younger than 400 Ma. The ellipses are results of multivariate estimation (robust Mahalanobis distance analysis; Campbell, 1980) that represents 95% of each of the subterrane data points. CHUR—chondrite uniform reservoir (Bouvier et al., 2008); DM—depleted mantle (Chauvel and Blichert-Toft, 2001). Data sources are: 1—this study; 2—George et al. (2021); 3—Romero et al. (2020); 4—Alberts et al. (2021); 5—Pecha et al. (2016); 6—Davis et al. (2015).

arc. The igneous zircons have lower Hf, and higher Yb and Nb relative to the detrital zircons (Fig. S11), and their slightly lower U/Yb values overlap the MORB-OIB–arc fields (Fig. 13). This could indicate an arc to backarc transition from the Carboniferous to the Permian. The chert deposits above the volcanic rocks support a change from active volcanism to relative quiescence and deep-water sedimentation (Cordey and Cornée, 2009).

The Origin of Stikinia

Belasky and Stevens (2006) modeled Permian fossil assemblages in the Stikine assemblage. They are dissimilar to North American assemblages, and they are not of the Tethyan realm. The assemblages share similarities with Eastern Klamath and Wrangel terranes, and Belasky and Stevens (2006) interpret that Permian Stikinia lies between Wrangellia (north) and East Klamath (south), ~2000–3000 km west of North America. The Carboniferous–Permian connection between Stikinia and Wrangellia is further strengthened by the comparison of detrital zircon results (Fig. 12). George et al. (2021) and Alberts et al. (2021) make similar comparisons, also including the Farewell terrane (Alaska), in this collage. They suggest that although these terranes may have accreted to the Laurentian margin at different times, in the Carboniferous to Permian, they constituted volcanic arcs isolated in the proto–Pacific Ocean (Fig. 14). The collective fossil assemblage modeling and zircon U/Pb-Hf results, with the addition of the trace-element interpretations herein (Figs. 11–13), support a Carboniferous to Permian chain of incipient ocean arcs that included Stikinia and Wrangellia and probably Quesnellia, Farewell, and East Klamath terranes (Fig. 14; Colpron and Nelson, 2011; Malkowski and Hampton, 2014; Alberts et al., 2021; Colpron and Nelson, 2021George et al., 2021). These terranes consistently contain minor populations of older detrital zircon; for example, ~5% of the detrital zircon in the Asitka Group are Paleoproterozoic. However, juvenile zircon εHf(t) compositions prohibit old continental crust in the early evolution of eastern Stikinia (Figs. 11 and 12). Whatever lithosphere contributed the ancient

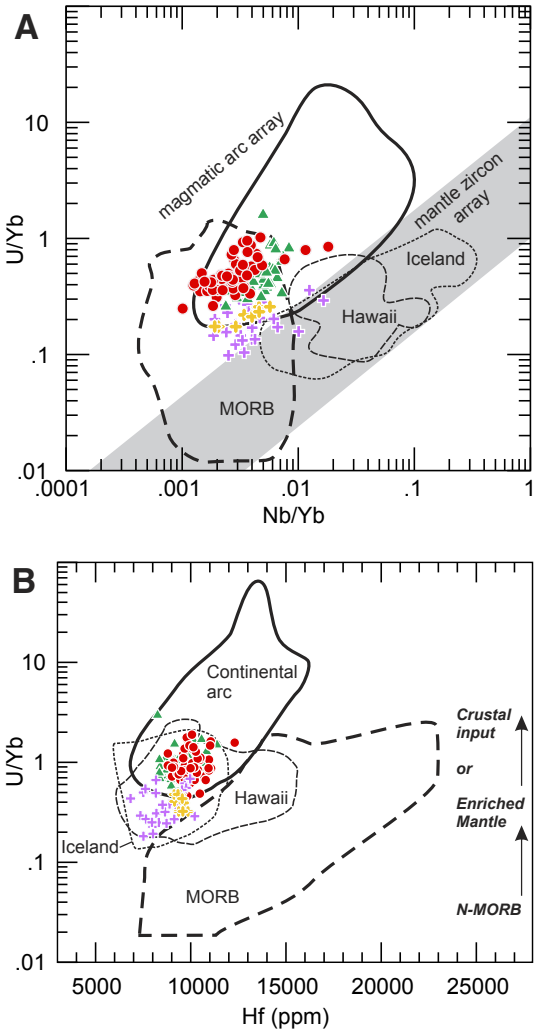

Figure 13. (A) Nb/Yb versus U/Yb and (B) Hf versus U/Yb for Asitka Group and Hazelton Group (Telkwa Formation) detrital zircons and Asitka Group igneous zircons. Discrimination fields are from Grimes et al. (2015). MORB—mid-ocean ridge basalt; N-MORB—normal mid-ocean ridge basalt.

zircons must have been a piece of continental crust in the oceanic domain. Further discovery and interrogation of early Paleozoic and Precambrian detrital zircons in these terranes will be essential to establish what preexisting continent these peripheral crustal fragments rifted and drifted from, and thereby in what realm they were born (e.g., Baltica versus Panthalassa).

The final contribution from our study is that the Hazelton Group (Telkwa Formation) of eastern Stikinia does not contain evidence of interaction with ancient crust. The Telkwa Formation zircons εHf(t) are most easily explained by derivation from juvenile magmatic rocks in an arc environment formed on the same oceanic lithosphere as the volcanosedimentary rocks of the Asitka Group and the picrites of the Stuhini Group (Figs. 11–13; Milidragovic et al., 2018). The Hazelton Group in western Stikinia does have a few ca. 200 Ma zircons (<5%) with more evolved εHf(t) (Figs. 11, 12B, and 12C; George et al., 2021). Overlooking potential analytical issues (e.g., mineral inclusions intersected during LA-ICP-MS, which should have been screened out on examination of the time-resolved signal traces), the more evolved εHf(t) indicates interaction with Neoproterozoic or older lithosphere. This lithosphere could be the yet undefined peripheral landmass that contributed the rare Precambrian detrital zircons. A preliminary interpretation by George et al. (2021), based on the age spectra of the rare pre-late Paleozoic detrital zircons, is that this landmass does not share affinity with western North America, and like the Alexander terrane, may have been derived from northern Panthalassa or Baltic realms (see Colpron and Nelson, 2011; Beranek et al., 2013). A second option is that the landmass was the Yukon-Tanana terrane, which became imbricated with Stikinia in the Late Triassic and contaminated Stuhini and Hazelton arc magmas. A final consideration is that although the Precambrian zircons constitute <5% in Stikinia, they represent a range of 1.5 billion years (Fig. 11B). The most plausible source of such a broad age range is one or more older sedimentary successions. For example, the Mackenzie Mountains and Shaler supergroups (Meso- to Neoproterozoic) were deposited in northwestern North America but were supplied by continental-scale river

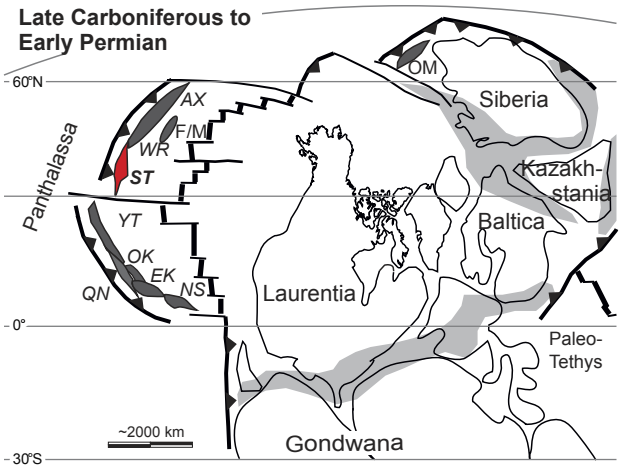

Figure 14. Carboniferous to Permian schematic paleogeographic reconstruction, modified from Nelson et al. (2013) and George et al. (2021). The Farewell/Mystic terrane is placed in the Panthalassic realm after Malkowski and Hampton (2014). We have separated Stikine from Yukon-Tanana terranes because the zircon evidence does not support that Yukon-Tanana was in the detrital source. AX—Alexander; EK—East Klamath; F/M—Farewell/Mystic; OK—Okanagan; OM—Omulevka; NS—northern Sierra terranes; QN—Quesnellia; ST—Stikinia; WR—Wrangellia; YT—Yukon-Tanana.

systems that drained the Grenville Province in eastern North America (Rainbird et al., 2017). These zircons were recycled into the rift-related Windermere Supergroup (Neoproterozoic) and Paleozoic passive margin sedimentary rocks (Cambrian Type 2 of Hadlari et al., 2012). Each of these stratigraphic units contains a pan-Laurentian zircon record. Such a peripheral landmass could explain the broad range of ages recorded in the Stikinian detrital zircons (Figs. 11D and 12).

The new data provide evidence that eastern Stikinia was born as an incipient arc in the Carboniferous (Fig. 14) and remained as oceanic crust with a peripheral crustal fragment until imbrication with another evolved terrane during the Late Triassic. The crustal fragment, its extent, and its birthplace remain to be determined.

CONCLUSIONS

We apply igneous and detrital zircon U/Pb-Hf and trace-element analysis to the Asitka Group and Hazelton Group (Telkwa Formation) in eastern Stikinia and complement this data set with radiolarian ages. The Asitka Group was deposited in a deep marine environment, and extracted radiolarians from cherts are only identified on the genus level but are typical of the assemblages *P. scalprata* m., *rhombothoracata*, and *Ruzhencevispongus uralicus*, which range from the Late Artinskian to the Late Kungurian. This is consistent with, albeit slightly younger than, U-Pb ages of two rhyolites (ca. 294 and 289 Ma). Detrital zircons from a rare sandstone unit, which is stratigraphically below the rhyolites, range from ca. 350–305 Ma with minor Paleoproterozoic zircons (5%). The Telkwa Formation detrital zircon yields a maximum deposition age of ca. 196 Ma.

The combined εHf(t) and trace-element compositions of zircon indicate that the Asitka Group was deposited on a Carboniferous juvenile oceanic arc during the early Permian. The zircon trace elements from rhyolites in this study have lower U/Yb than the detrital zircons, potentially indicating evolution to a backarc-like setting from Carboniferous to Permian. The Telkwa Formation detrital zircon trace elements are also consistent with an arc-like environment. The zircon εHf(t) provide no evidence of old basement in the magmatic sources in eastern Stikinia, and the contribution of the Paleoproterozoic zircon to the Asitka Group sandstone must have come from a peripheral continental landmass. This landmass may have been imbricated with western Stikinia in the Late Triassic, but our study provides no evidence of its existence in eastern Stikinia, which was born and evolved from the ocean floor. Multivariate statistical evaluation of the U/Pb-Hf systematics of detrital zircons from the Asitka Group shows a remarkable overlap with Wrangellia, particularly in Alaska. Although these terranes collided with North America at different times, the similar zircon age and chemistry are consistent with published fossil modeling that pairs Stikinia and Wrangellia as volcanic arcs isolated in the proto–Pacific Ocean during the Carboniferous and Permian.

ACKNOWLEDGMENTS

This study is a contribution to the Hogem mapping project by the British Columbia Geological Survey. Field assistance was provided by K. Shortridge, M. Farhat, and J. Lockie. Clémentine Fellah (Laboratoire de Géologie de Lyon) assisted with the radiolarian SEM session. T. Ockerman and K. Gordon (PCIGR) conducted the igneous zircon Hf isotopic analyses. F. Cordey is supported by the Centre National de la Recherche Scientifique (CNRS), France, Unité Mixte de Recherche UMR 5276. This is Natural Resources Canada contribution #20210338. Discussions with colleagues at the British Columbia Geological Survey improved our understanding of Stikinia, and S. George and an anonymous reviewer helped improve the manuscript.

REFERENCES CITED

Aitchison, J.C., Suzuki, N., Caridroit, M., Danelian, T., and Noble, P., 2017, Paleozoic radiolarian biostratigraphy: Geodiversitas, v. 39, no. 3, p. 503–531, https://doi.org/10.5252/g2017n3a5.

Alberts, D., Gehrels, G.E., and Nelson, J., 2021, U-Pb and Hf analyses of detrital zircons from Paleozoic and Cretaceous strata on Vancouver Island, British Columbia: Constraints on the Paleozoic tectonic evolution of southern Wrangellia: Lithosphere, v. 2021, no. 1, https://doi.org/10.2113/2021/7866944.

Barresi, T., Nelson, J.L., Dostal, J., and Friedman, R., 2015, Evolution of the Hazelton arc near Terrace, British Columbia: Stratigraphic, geochronological, and geochemical constraints on a Late Triassic–Early Jurassic arc and Cu-Au porphyry belt: Canadian Journal of Earth Sciences, v. 52, p. 466–494, https://doi.org/10.1139/cjes-2014-0155.

Belasky, P., and Stevens, C.H., 2006, Permian faunas of westernmost North America: Paleobiogeographic constraints on Permian positions of Cordilleran terrane, *in* Haggart, W., Rankin, R.J., and Monger, J.W.H., eds., Paleogeography of the North American Cordillera: Evidence for and against Large-Scale Displacements: Geological Association of Canada Special Paper 46, p. 71–80.

Beranek, L.P., van Staal, C.R., McClelland, W.C., Israel, S., and Mihalynuk, M.G., 2013, Baltican crustal provenance for Cambrian–Ordovician sandstones of the Alexander terrane, North American Cordillera: Evidence from detrital zircon U-Pb geochronology and Hf isotope geochemistry: Journal

of the Geological Society of London, v. 170, p. 7–18, https://doi.org/10.1144/jgs2012-028.
Bouvier, A., Vervoort, J.D., and Patchett, J.P., 2008, The Lu-Hf and Sm-Nd isotopic composition of CHUR: Constraints from unequilibrated chondrites and implications for the bulk composition of terrestrial planets: Earth and Planetary Science Letters, v. 273, p. 48–57, https://doi.org/10.1016/j.epsl.2008.06.010.
Brown, D.A., Logan, J.M., Gunning, M.H., Orchard, M.J., and Bamber, W.E., 1991, Stratigraphic evolution of the Paleozoic Stikine assemblage in the Stikine and Iskut rivers area, northwestern British Columbia: Canadian Journal of Earth Sciences, v. 28, p. 958–972, https://doi.org/10.1139/e91-087.
Brown, D.A., Gunning, M.H., and Greig, C.J., 1996, The Stikine project: Geology of western Telegraph Creek map area, northwestern British Columbia: British Columbia Geological Survey, Ministry of Energy, Mines and Petroleum Resources Bulletin 95, 183 p.
Campbell, N.A., 1980, Robust procedures in multivariate analysis. I: Robust covariance estimation: Applied Statistics, v. 29, p. 231–237, https://doi.org/10.2307/2346896.
Chauvel, C., and Blichert-Toft, J., 2001, A hafnium isotope and trace element perspective on melting of the depleted mantle: Earth and Planetary Science Letters, v. 190, p. 137–151, https://doi.org/10.1016/S0012-821X(01)00379-X.
Cohen, K.M., Finney, S.C., Gibbard, P.L., and Fan, J.-X., 2013, The ICS International Chronostratigraphic Chart: Episodes, v. 36, p. 199–204, https://doi.org/10.18814/epiiugs/2013/v36i3/002.
Colpron, M., 2020, Yukon Terranes—A digital atlas of terranes for the northern Cordillera: Yukon Geological Survey, http://data.geology.gov.yk.ca/Compilation/2 (accessed April 2021).
Colpron, M., and Nelson, J.L., 2011, A Palaeozoic NW Passage and the Timanian, Caledonian and Uralian connections of some exotic terranes in the North American Cordillera, *in* Spencer, A.M., Embry, A.F., Gautier, D.L., Stoupakova, A.V., and Sørensen, K., eds., Arctic Petroleum Geology: Geological Society of London Memoir 35, p. 463–484, https://doi.org/10.1144/M35.31.
Colpron, M., and Nelson, J.L., 2021, Northern Cordillera: Canada and Alaska, *in* Selley, R.C, Robin, L., Cocks, M., and Plimer, I.R., eds., North America: Northern Cordillera: Encyclopedia of Geology: Elsevier Ltd., p. 93–106.
Colpron, M., Nelson, J.L., and Murphy, D.C., 2007, Northern Cordilleran terranes and their interactions through time: GSA Today, v. 17, no. 4/5, p. 4–10, https://doi.org/10.1130/GSAT01704-5A.1.
Colpron, M., Crowley, J.L., Long, D.G.F., Murphy, D.C., Beranek, L., and Bickerton, L., 2015, Birth of the northern Cordilleran orogen, as recorded by detrital zircons in Jurassic synorogenic strata and regional exhumation in Yukon: Lithosphere, v. 7, p. 541–562, https://doi.org/10.1130/L451.1.
Cordey, F., and Cornée, J.J., 2009, New radiolarian assemblages from La Desirade Island basement complex (Guadeloupe, Lesser Antilles arc) and Caribbean tectonic implications: Bulletin de la Société Géologique de France, v. 180, p. 399–409, https://doi.org/10.2113/gssgfbull.180.5.399.
Cordey, F., and Krauss, P., 1990, A field technique for identifying and dating radiolaria applied to British Columbia and Yukon, *in* Current Research, Part E: Cordillere et Marge du Pacifique: Geological Survey of Canada Paper 90-1E, p. 127–129, https://doi.org/10.4095/131378.
Coutts, D.S., Matthews, W.A., and Hubbard, S.M., 2019, Assessment of widely used methods to derive depositional ages from detrital zircon populations: Geoscience Frontiers, v. 10, p. 1421–1435, https://doi.org/10.1016/j.gsf.2018.11.002.
Currie, L., and Parrish, R.R., 1993, Jurassic accretion of Nisling terrane along the western margin of Stikinia, Coast Mountains, northwestern British Columbia: Geology, v. 21, p. 235–238, https://doi.org/10.1130/0091-7613(1993)021<0235:JAONTA>2.3.CO;2.
Davis, W.J., Ootes, L., Newton, L., Jackson, V.A., and Stern, R., 2015, Characterization of the Paleoproterozoic Hottah terrane, Wopmay Orogen using multi-isotopic (U-Pb, Hf and O) detrital zircon analyses: An evaluation of linkages to northwest Laurentian Paleoproterozoic domains: Precambrian Research, v. 269, p. 296–310, https://doi.org/10.1016/j.precamres.2015.08.012.
Diakow, L.J., 2001, Geology of the southern Toodoggone River and northern McConnell Creek map areas, north-central British Columbia: Parts of NTS 94E/2, 94D/15 and 94D/16: British Columbia Geological Survey, Ministry of Energy and Mines Geoscience Map 2001-1, scale 1:50,000.
Evenchick, C.A., Mustard, P.S., McMechan, M., Ferri, F., Porter, S., Hadlari, T., and Jakobs, G., 2007, Geology, McConnell Creek, British Columbia: Geological Survey of Canada Open-File 5571, British Columbia Ministry of Energy, Mines and Petroleum Resources, Petroleum Geology Open File 2007-10, scale 1:125,000.
Gagnon, J.-F., Barresi, T., Waldon, J.W.F., Nelson, J.L., Poulton, T.P., and Cordey, F., 2012, Stratigraphy of the upper Hazelton Group and the Jurassic evolution of the Stikine terrane, British Columbia: Canadian Journal of Earth Sciences, v. 49, p. 1027–1052, https://doi.org/10.1139/e2012-042.
Galbraith, R.F., 1994, Some applications of radial plots: Journal of the American Statistical Association, v. 89, p. 1232–1242, https://doi.org/10.1080/01621459.1994.10476864.
George, S.W.M., Nelson, J.L., Alberts, D., Greig, C.J., and Gehrels, G.E., 2021, Triassic–Jurassic accretionary history and tectonic origin of Stikinia from U-Pb geochronology and Lu-Hf isotope analysis, British Columbia: Tectonics, v. 40, https://doi.org/10.1029/2020TC006505.
Golding, M.L., 2020, Evaluating tectonic models for the formation of the North American Cordillera using multivariate statistical analysis of Late Triassic conodont faunas: Palaeobiodiversity and Palaeoenvironments, v. 100, p. 135–149, https://doi.org/10.1007/s12549-019-00393-4.
Goolaerts, A., Mattielli, N., De Jong, J.T.M., Weis, D., and Scoates, J., 2004, Hf and Lu isotopic reference values for the zircon standard 91500 by MC-ICP-MS: Chemical Geology, v. 206, p. 1–9, https://doi.org/10.1016/j.chemgeo.2004.01.008.
Greig, C.J., Dudek, N.P., ver Hoeve, T.J., Newton, G., and Greig, R.E., 2021, Geology of the Tatogga property: Geologic framework for the Saddle North porphyry Cu-Au deposit and the Saddle South epithermal Au-Ag vein system, Iskut district, northwestern British Columbia, *in* Geological Fieldwork 2020: British Columbia Ministry of Energy, Mines and Low Carbon Innovation: British Columbia Geological Survey Paper 2021-01, p. 89–111.
Grimes, C.B., Wooden, J.L., Cheadle, M.J., and John, B.E., 2015, "Fingerprinting" tectono-magmatic provenance using trace elements in igneous zircon: Contributions to Mineralogy and Petrology, v. 170, https://doi.org/10.1007/s00410-015-1199-3.
Gunning, M.H., Fedeorowski, J., and Bamber, E.W., 2006a, Paleogeographic significance of mid-Carboniferous limestone, northwestern Sitkine terrane, British Columbia, *in* Haggart, W., Rankin, R.J., and Monger, J.W.H., eds., Paleogeography of the North American Cordillera: Evidence for and against Large-Scale Displacements: Geological Association of Canada Special Paper 46, p. 59–69.
Gunning, M.H., Hodder, R.W.H., and Nelson, J.L., 2006b, Contrasting volcanic styles within the Paleozoic Stikine assemblage, western Stikine terrane, northwestern British Columbia, *in* Colpron, M., and Nelson, J.L., eds., Paleozoic Evolution and Metallogeny of Pericratonic Terranes at the Ancient Pacific Margin of North America, Canadian and Alaskan Cordillera.: Geological Association of Canada Special Paper 45, p. 201–227.
Gunning, M.H., Bamber, E.W., Anderson, R.G., Fedeorowski, J., Friedman, R., Mamet, B.L., Orchard, M.J., Rui, L., and Mortensen, J.K., 2007, The mid-Carboniferous Arctic Lake Formation, northwestern Stikine terrane, British Columbia: Bulletin of Canadian Petroleum Geology, v. 55, p. 21–50, https://doi.org/10.2113/gscpgbull.55.1.21.
Hadlari, T., Davis, W.J., Dewing, K., Heaman, L.M., Lemieux, Y., Ootes, L., Pratt, B.R., and Pyle, L.J., 2012, Two detrital zircon signatures for the Cambrian passive margin of northern Laurentia highlighted by new U-Pb results from northern Canada: Geological Society of America Bulletin, v. 124, p. 1155–1168, https://doi.org/10.1130/B30530.1.
Herriott, T.M., Crowley, J.L., Schmitz, M.D., Wartes, M.A., and Gillis, R.J., 2019, Exploring the law of detrital zircon: LA-ICP-MS and CA-TIMS geochronology of Jurassic forearc strata, Cook Inlet, Alaska, USA: Geology, v. 47, p. 1044–1048, https://doi.org/10.1130/G46312.1.
Irving, E., and Monger, J.W.H., 1987, Preliminary paleomagnetic results from the Permian Asitka Group, British Columbia: Canadian Journal of Earth Sciences, v. 24, p. 1490–1497, https://doi.org/10.1139/e87-141.
Jackson, J.L., Gehrels, G.E., Patchett, P.J., and Mihalynuk, M.G., 1991, Stratigraphic and isotopic link between the northern Stikine terrane and an ancient continental margin assemblage, Canadian Cordillera: Geology, v. 19, p. 1177–1180, https://doi.org/10.1130/0091-7613(1991)019<1177:SAILBT>2.3.CO;2.
Logan, J.M., and Mihalynuk, M.G., 2014, Tectonic controls on early Mesozoic paired alkaline porphyry deposit belts (Cu-Au ± Ag-Pt-Pd-Mo) within the Canadian Cordillera: Economic Geology, v. 109, p. 827–858, https://doi.org/10.2113/econgeo.109.4.827.
Logan, J.M., Drobe, J.R., and McClelland, W.C., 2000, Geology of the Forrest Kerr–Mess Creek area, northwest British Columbia (NTS 104/B10, 15 & 104G/2 &7W): British Columbia Geological Survey, Ministry of Energy and Mines Bulletin 104, 178 p.
Lord, C.S., 1948, McConnell Creek map-area, Cassiar District, British Columbia: Geological Survey of Canada Memoir 251, 82 p., https://doi.org/10.4095/101588.
Ludwig, K.R., 2003, Isoplot 3.00, A Geochronological Toolkit for Microsoft Excel: Berkeley Geochronology Center Special Publication 4: Berkeley, California, 74 p.

Malkowski, M.A., and Hampton, B.A., 2014, Sedimentology, U-Pb detrital geochronology, and Hf isotopic analyses from Mississippian–Permian stratigraphy of the Mystic subterrane, Farewell terrane, Alaska: Lithosphere, v. 6, p. 383–398, https://doi.org/10.1130/L365.1.

Marsden, H., and Thorkelson, D.J., 1992, Geology of the Hazelton volcanic belt in British Columbia: Implications for the Early to Middle Jurassic evolution of Stikinia: Tectonics, v. 11, p. 1266–1287, https://doi.org/10.1029/92TC00276.

Mattinson, J.M., 2005, Zircon U-Pb chemical abrasion ("CA-TIMS") method: Combined annealing and multi-step partial dissolution analysis for improved precision and accuracy of zircon ages: Chemical Geology, v. 220, p. 47–66, https://doi.org/10.1016/j.chemgeo.2005.03.011.

McClelland, W.C., 1992, Permian and older rocks of the southwestern Iskut River map area, northwestern British Columbia, *in* Current Research: Geological Survey of Canada Paper 92-IA, p. 303–307.

Mihalynuk, M.G., 1999, Geology and mineral resources of the Tagish Lake area (NTS 104M/8, 9, 10E, 15 and 104N/12W) northwestern British Columbia: British Columbia Geological Survey, Ministry of Energy and Mines Bulletin 105, 217 p.

Mihalynuk, M.G., Nelson, J.L., and Diakow, L.J., 1994, Cache Creek terrane: Oroclinal paradox within the Canadian Cordillera: Tectonics, v. 13, p. 575–595, https://doi.org/10.1029/93TC03492.

Milidragovic, D., Zagorevski, A., Weis, D., Joyce, N., and Chapman, J.B., 2018, Picrite "Intelligence" from the Middle-Late Triassic Stikine arc: Composition of mantle wedge asthenosphere: Lithos, v. 308–309, p. 446–461, https://doi.org/10.1016/j.lithos.2018.03.014.

Miller, E.A., Kennedy, L.A., and van Straaten, B.I., 2020, Geology of the Kinskuch Lake area and Big Bulk porphyry prospect, northwestern British Columbia: Syndepositional faulting and basin formation during the Rhaetian (latest Triassic) transition from the Stuhini to the Hazelton Group, *in* Geological Fieldwork 2019: British Columbia Ministry of Energy, Mines and Petroleum Resources, British Columbia Geological Survey Paper 2020-01, p. 77–99.

Monger, J.W.H., 1977, The Triassic Takla Group in McConnell Creek map-area, north-central British Columbia: Geological Survey of Canada Paper 76-29, 45 p., https://doi.org/10.4095/102634.

Monger, J.W.H., and Church, B.N., 1977, Revised stratigraphy of the Takla Group, north-central British Columbia: Canadian Journal of Earth Sciences, v. 14, no. 2, p. 318–326, https://doi.org/10.1139/e77-031.

Monger, J.W.H., and Irving, E., 1980, Northward displacement of north-central British Columbia: Nature, v. 285, p. 289–294, https://doi.org/10.1038/285289a0.

Monger, J.W.H., Price, R.A., and Templeman-Kluit, D.J., 1982, Tectonic accretion and the origin of the two major metamorphic and plutonic welts in the Canadian Cordillera: Geology, v. 10, p. 70–75, https://doi.org/10.1130/0091-7613(1982)10<70:TAATOO>2.0.CO;2.

Mundil, R., Ludwig, K.R., Metcalfe, I., and Renne, P.R., 2004, Age and timing of the Permian mass extinctions: U/Pb dating of closed-system zircons: Science, v. 305, p. 1760–1763, https://doi.org/10.1126/science.1101012.

Nelson, J., Waldron, J., van Straaten, B., Zagoresvski, A., and Rees, C., 2018, Revised stratigraphy of the Hazelton Group in the Iskut River region, northwestern British Columbia, *in* Geological Fieldwork 2017: British Columbia Ministry of Energy, Mines and Petroleum Resources, British Columbia Geological Survey Paper 2018-1, p. 15–38.

Nelson, J.L., Colpron, M., and Israel, S., 2013, The Cordillera of British Columbia, Yukon, and Alaska, *in* Colpron, M., Bissig, T., Rusk, B.G., and Thompson, J.F.H., eds., Tectonics and Metallogeny in Tectonics, Metallogeny, and Discovery: The North American Cordillera and Similar Accretionary Settings: Society of Economic Geologists Special Publication 17, p. 53–109.

Ootes, L., Bergen, A.L., Milidragovic, D., and Jones, G.O., 2020a, Bedrock geology of the northern Hogem batholith and its surroundings, north-central British Columbia: British Columbia Ministry of Energy and Mines and Petroleum Resources, British Columbia Geological Survey Open File 2020-02, scale 1:50,000.

Ootes, L., Bergen, A.L., Milidragovic, D., Jones, G.O., Camacho, A., and Friedman, R., 2020b, An update on the geology of northern Hogem batholith and its surroundings, north-central British Columbia, *in* Geological Fieldwork 2019: British Columbia Ministry of Energy, Mines and Petroleum Resources, British Columbia Geological Survey Paper 2020-01, p. 25–47.

Ootes, L., Jones, G., Schiarizza, P., Milidragovic, D., Friedman, R., Camacho, A., Luo, Y., Vezinet, A., Pearson, D.G., and Zhang, S., 2020c, Geochronologic and geochemical data from northern Hogem batholith and its surroundings, north-central British Columbia: British Columbia Ministry of Energy, Mines and Petroleum Resources, British Columbia Geological Survey Geofile 2020-01, 25 p., digital files.

Pecha, M.E., Gehrels, G.E., McClelland, W.C., Giesler, D., White, C., and Yokelson, I., 2016, Detrital zircon U-Pb geochronology and Hf isotope geochemistry of the Yukon-Tanana terrane, Coast Mountains, southeast Alaska: Geosphere, v. 12, no. 5, p. 1556–1574, https://doi.org/10.1130/GES01303.1.

Rainbird, R.H., Rayner, N.M., Hadlari, T., Heaman, L.M., Ielpi, A., Turner, E.C., and MacNaughton, R.B., 2017, Zircon provenance data record the lateral extent of pancontinental, early Neoproterozoic rivers and erosional unroofing history of the Grenville orogen: Geological Society of America Bulletin, v. 129, p. 1408–1423, https://doi.org/10.1130/B31695.1.

Richards, T.A., 1976, McConnell Creek map-area (94D), east half, British Columbia: Geological Survey of Canada Paper 76-IA, p. 43–50.

Rigby, J.K., 1973, Permian sponges from western British Columbia: Canadian Journal of Earth Sciences, v. 10, p. 1600–1606, https://doi.org/10.1139/e73-153.

Romero, M.C., Ridgwah, K.D., and Gehrels, G.E., 2020, Geology, U-Pb geochronology, and Hf isotope geochemistry across the Mesozoic Alaska Range Suture Zone (south-central Alaska): Implications for Cordilleran collisional processes and tectonic growth of North America: Tectonics, v. 39, https://doi.org/10.1029/2019TC005946.

Ross, C.A., and Monger, J.W.H., 1978, Carboniferous and Permian Fusulinaceans from the Omineca Mountains, British Columbia, *in* Donnelly, V., ed., Contributions to Canadian Paleontology: Geological Survey of Canada Bulletin 267, p. 43–63.

Scoates, J.S., and Friedman, R.M., 2008, Precise age of the platinuferous Merensky Reef, Bushveld Complex, South Africa, by the U-Pb ID-TIMS chemical abrasion technique: Economic Geology, v. 103, no. 3, p. 465–471, https://doi.org/10.2113/gsecongeo.103.3.465.

Sun, S.S., and McDonough, W.F., 1989, Chemical and isotopic systematics of oceanic basalts: Implications for mantle composition and processes, *in* Saunders, A.D., and Norry, M.J., eds., Magmatism in the Ocean Basins: Geological Society of London Special Publication 42, p. 313–345, https://doi.org/10.1144/GSL.SP.1989.042.01.19.

Thorkelson, D.J., Mortensen, J.K., Marsden, H., and Taylor, R.P., 1995, Age and tectonic setting of Early Jurassic episodic volcanism along the northeastern margin of the Hazelton trough, northern British Columbia, *in* Miller, D.M., and Busby, C., eds., Jurassic Magmatism and Tectonics of the North American Cordillera: Geological Society of America Special Paper 299, p. 83–94, https://doi.org/10.1130/SPE299-p83.

Tipper, H.W., and Richards, T.A., 1976, Jurassic stratigraphy and history of north-central British Columbia: Geological Survey of Canada, Bulletin 270, 73 p., https://doi.org/10.4095/103065.

Vermeesch, P., 2018, IsoplotR: A free and open toolbox for geochronology: Geoscience Frontiers, v. 9, p. 1479–1493, https://doi.org/10.1016/j.gsf.2018.04.001.

Weis, D., Kieffer, B., Hanano, D., Barling, J., Pretorius, W., Maerschalk, C., and Mattielli, M., 2007, Hf isotope compositions of U.S. Geological Survey reference materials: Geochemistry, Geophysics, Geosystems, v. 8, Q06006, https://doi.org/10.1029/2006GC001473.